JGR Planets

Key Points:

- The upper mesosphere of Venus can be supersaturated with respect to both amorphous solid water (ASW) and crystalline carbon dioxide ice
- There is a persistent layer of nano-scale ASW particles encircling Venus
- Short-lived carbon dioxide ice clouds may sporadically form in the upper mesosphere

Correspondence to:

B. J. Murray,
b.j.murray@leeds.ac.uk

Ephemeral Ice Clouds in the Upper Mesosphere of Venus

Benjamin. J. Murray[1] , **Thomas. P. Mangan**[2] , **Anni Määttänen**[3] , and **John. M. C. Plane**[2]

[1]School of Earth and Environment, University of Leeds, Leeds, UK, [2]School of Chemistry, University of Leeds, Leeds, UK, [3]LATMOS/IPSL, Sorbonne Université, UVSQ Université Paris-Saclay, CNRS, Paris, France

Abstract The conditions in Venus' upper mesosphere at around 120 km have some similarities to the upper mesosphere of Earth and Mars where ice clouds form. Here we show, using published satellite products and numerical modeling, that the upper mesosphere of Venus can be sufficiently cold that both H_2O and CO_2 may condense to form particles. We show that amorphous solid water particles (ASW) are likely to nucleate both heterogeneously on meteoric smoke and also homogeneously, resulting in clouds of nano-scaled particles at around 120 km that will occur globally. The temperatures may then become sufficiently low, below ∼90 K, that CO_2 particles can nucleate on ASW particles. Given the uncertainty associated with retrievals of temperature in the upper mesosphere, it is unclear how frequently this occurs, but it could be >30% of the time poleward of 60°. Since the main component of Venus' tenuous atmosphere is CO_2, any CO_2 crystals that form will grow and sediment on a timescale of 10–20 min. Mie calculations show that these Venusian mesospheric clouds (VMCs) should be observable by contemporary satellite instruments, although their short lifetime means that the probability of detection is small. We suggest that VMCs are important for the redistribution of meteoric smoke and may serve as a cold-trap, removing some water vapor from the very upper mesosphere of Venus through the growth and sedimentation of cloud particles, and possibly reducing the loss of water to space.

Plain Language Summary Venus is renowned for extreme heat at the surface and clouds composed of sulfuric acid encircling the planet; however, there are regions of Venus's atmosphere that are sufficiently cold to harbor ice clouds. In fact, the temperatures frequently fall below 100 K at around 120 km altitude and under the right conditions, we have shown that ice clouds composed of both water and carbon dioxide ices can form. We have used published data from satellites that orbit Venus to show that clouds composed of nanometer sized water ice particles may encircle the planet. The temperatures are so low in this part of Venus' atmosphere that the ice in these water ice particles likely lacks any crystalline structure, i.e., it has an amorphous (liquid-like) structure. Furthermore, if the temperature falls below about 90 K, we have shown that carbon dioxide ice crystals can form on top of water ice particles. Since the atmosphere of Venus is mainly made of carbon dioxide, these carbon dioxide crystals grow and then sediment rapidly in the thin atmosphere. If we were lucky enough to see one of these short-lived sporadic clouds, it would look a bit like mares' tail cloud on Earth.

1. Introduction

The plausibility of ice clouds in Venus' atmosphere has been discussed as early as the 1950s (Menzel & Whipple, 1954). Through differing analyses of infrared absorption seen at 3 μm from high altitude balloon measurements in the 1960s, both Bottema et al. (1965) and Pollack and Sagan (1968) suggested water ice clouds could explain the observed absorbances, although a rebuttal by Rea and O'Leary (1968) suggested this was possible only if the ice particles were submicron in size. Turco et al. (1983) expanded on these predictions, suggesting that water ice clouds may be present in two layers: one between 80 and 100 km, resulting from freezing of sulfuric acid haze droplets; and another layer at Venus' mesopause (∼120 km) consisting of water ice nanoparticles, possibly nucleated on meteoric dust particles.

Since the prediction of water ice clouds on Venus by Turco et al. (1983), our understanding of both the physics of ice cloud formation in planetary atmospheres and the structure and dynamics of the Venusian atmosphere has increased greatly. A range of satellite observations of lower altitude (≤100 km) sulfuric acid haze layers have since been made (Limaye et al., 2018; Titov et al., 2018), and recent observations by instruments onboard the Venus Express satellite have highlighted extreme temperature minima in Venus' upper atmosphere (Mahieux et al., 2015, 2023).
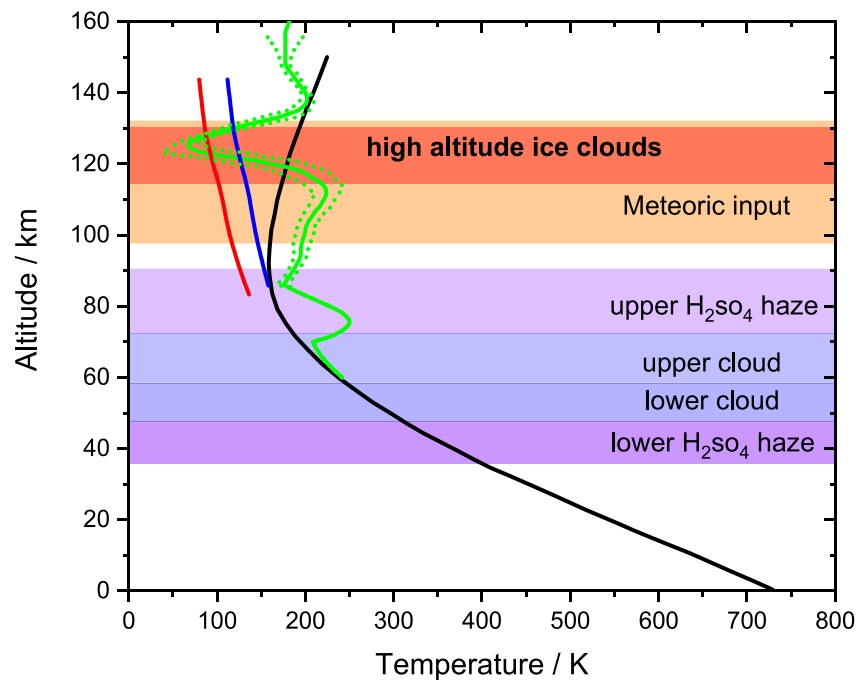
Figure 1. Atmosphere of Venus showing known and proposed cloud layers. General atmospheric profile (black) extracted from Palen et al. (2019). The Solar Occultation in the InfraRed temperature profile from orbit 669.1 (green) together with quoted uncertainty is taken from Mahieux et al. (2015). Saturation temperatures shown for H_2O with respect to amorphous solid water (ASW) (blue) and CO_2 with respect to crystalline CO_2 (red). The water saturation ratios were calculated using the Nachbar et al. (2019) parameterization for ASW in combination with the vapor pressure over hexagonal ice (Murphy & Koop, 2005). The frost point for crystalline CO_2 ice was calculated using saturation vapor pressure parameterization from Azreg-Aïnou (2005). The altitude range over which meteoric ablation occurs is taken from Carrillo-Sánchez et al. (2020).

Figure 1 illustrates an example of a typical cold temperature profile (green line) from the Solar Occultation in the InfraRed (SOIR) instrument onboard the Venus Express satellite (Orbit 669.1, taken at 81.6° latitude on the 19 February 2008 from Mahieux et al. (2015)). The temperature 125 km is at a minimum value of 67 ± 20 K, with the region between about 123 and 128 km being below 100 K. The blue line in Figure 1 shows the saturation temperature for H_2O with respect to amorphous solid water (ASW), assuming a water vapor concentration of 1 ppmv (the expected range in the Venusian upper atmosphere is 0.56–2.45 ppmv (Chamberlain et al., 2020)). This highlights that the atmosphere is sometimes significantly supersaturated with respect to ASW within the cold pocket. We show here the saturation (frost) point associated with ASW rather than the stable crystalline hexagonal phase of ice I (ice I_h) because under these conditions in the upper atmosphere any ice formed should be amorphous (Mangan et al., 2021). The Turco et al. (1983) prediction of water ice clouds was based on an assumed water vapor concentration of 10 ppm at slightly lower altitudes than the example shown in Figure 1 but with a much higher temperature minimum of 110 K; this led to many orders of magnitude smaller supersaturations than those shown in Figure 1. These atmospheric conditions for water ice clouds evoke comparisons to Polar Mesospheric Clouds on Earth (Plane et al., 2015), and water ice clouds observed in the upper atmosphere of Mars (Stcherbinine et al., 2020). On Mars, upper mesospheric clouds are also thought to redistribute H_2O, although the process is not as effective as it might be if the growth of ice particles can quench the supersaturation (Fedorova et al., 2020); nevertheless, ice cloud formation and sedimentation of ice crystals will limit the amount of water transported vertically.

Figure 1 also shows the saturation temperature for crystalline CO_2 ice (phase I), the phase that we expect cloud particles to be composed of under conditions in the upper mesosphere of Venus (Mangan, Salzmann, et al., 2017), even if nucleation occurs through a different phase. The primarily CO_2 atmosphere of Venus is sufficiently dense and the cold pocket sufficiently cold that the atmosphere is also supersaturated with respect to CO_2 ice around the temperature minimum at 125 km. These atmospheric conditions are again comparable to the Martian upper atmosphere, where gravity wave-induced cold pockets enable the deposition of the primary atmospheric constituent, producing populations of micron-sized CO_2 ice particles (Listowski et al., 2014; Plane et al., 2018).

At the time of Turco et al. (1983), CO_2 ice clouds were not considered as a possibility, given that the first confirmed observations of high-altitude CO_2 ice clouds on Mars were not made for another 20 years (Montmessin et al., 2006), and the temperature minima reported by Turco et al. (1983) were insufficient to produce supersaturated conditions with respect to CO_2 ice.

Despite being higher on Venus, if H_2O and/or CO_2 ice clouds formed around this temperature minimum, they would exist in a region with striking similarities to the mesospheric clouds observed on Mars, quite possibly with similar nucleating particles available. Hence, building on the predictions of water ice clouds by Turco et al. (1983), we propose that ice clouds composed of both H_2O and CO_2 ice may form in Venus' upper atmosphere at around 115–130 km in altitude. In this paper, using the more extensive database of measurements for the Venus atmosphere that is now available, and applying our improved knowledge of high-altitude clouds on Earth and Mars, we examine the formation, growth and composition of H_2O and CO_2 ice clouds, and their detectability, in the upper atmosphere of Venus.

2. Nucleation of H_2O and CO_2 Particles in Venus' Mesosphere

To evaluate the feasibility of nucleation of H_2O and CO_2 ice particles in Venus' upper atmosphere, we employ two theoretical approaches: Classical Nucleation Theory (CNT) and Kinetic Nucleation Theory (KNT). Atmospheres can exist in a metastable state where the partial pressure of some condensable component is greater than the equilibrium vapor pressure of a condensed phase (or phases) (Murray & Jensen, 2010). Atmospheres can persist in a supersaturated state because there is a free energy barrier to nucleation of a new phase related to the creation of a new interface. Nucleation can either occur spontaneously (homogeneous nucleation) or occur at lower supersaturations on the surface of suitable particles. These ice-nucleating particles (INPs) stabilize the cluster of the condensed phase through favorable interactions with the surface. In clouds in the Earth's mesosphere (Murray & Jensen, 2010), there is thought to be a competition between homogeneous and heterogeneous nucleation, and the balance between the mechanism results in clouds with very different hydrometeor size distributions. Sometimes heterogeneous nucleation occurring at lower supersaturations than those required for homogeneous nucleation leads to the depletion of the supersaturation as the ice particles grow, thus preventing homogeneous nucleation from occurring. But, if the cooling rate is sufficiently rapid, then homogeneous as well as heterogeneous nucleation can occur (Murray & Jensen, 2010).

In the upper mesosphere of Venus, there are at least two condensable materials, CO_2 and H_2O. The stable form of both of these materials is crystalline under the conditions on Venus, but it is unlikely that the critical cluster is made up of the stable phase. In many nucleating systems the initial phase to nucleate is a metastable phase that has a smaller surface energy penalty than the stable phase (Mullin, 2001). The metastable phase may subsequently relax to the stable phase. In the case of water homogeneously nucleating from water vapor, laboratory measurements clearly show that it is the liquid phase that nucleates at temperatures below 200 K, even though the liquid phase rapidly converts to crystalline ice under those conditions (Wölk et al., 2013). At around 120 K, the deposition of water on surface results in ASW; hence, the nucleating phase was probably amorphous but at these low temperatures the kinetics of transformation to the stable phase were too slow for it to occur on the experimental time scale (mins-hours) (Duft et al., 2019; Mangan et al., 2021). Similarly, for CO_2, recent experiments and molecular dynamics studies show that the initial phase to nucleate is a liquid-like form of CO_2 between 75 and 92 K (Dingilian et al., 2020; Halonen et al., 2021).

Heterogeneous nucleation requires the presence of particles on which nucleation might occur. The most likely candidate for particles that might serve as INPs for ice clouds on Venus are nm-sized Meteoric Smoke Particles (MSPs). MSPs form from the recondensation of metallic compounds (oxides, hydroxides, and carbonates) formed from the ablation of metals such as Fe, Mg, and Na from cosmic dust particles entering oxidizing planetary atmosphere such as Venus (Plane et al., 2015). Current predictions for Venus by Carrillo-Sánchez et al. (2020) show that ablation should occur between 100 and 130 km, peaking around 115 km (Figure 1). This altitude range coincides with the cold pocket (Figure 1). In the following sections, we use CNT and KNT to test the likelihood of both homogeneous and heterogeneous nucleation of both CO_2 and H_2O particles in the upper mesosphere of Venus. Note that there are also significant concentrations of HCl in Venus' upper mesosphere, approaching 1 ppm around 110 km and therefore ∼1%–10% of the H_2O mixing ratio (Mahieux et al., 2015). HCl may therefore play a role as a condensable vapor, though this is likely to be a minor enhancement of that of H_2O.
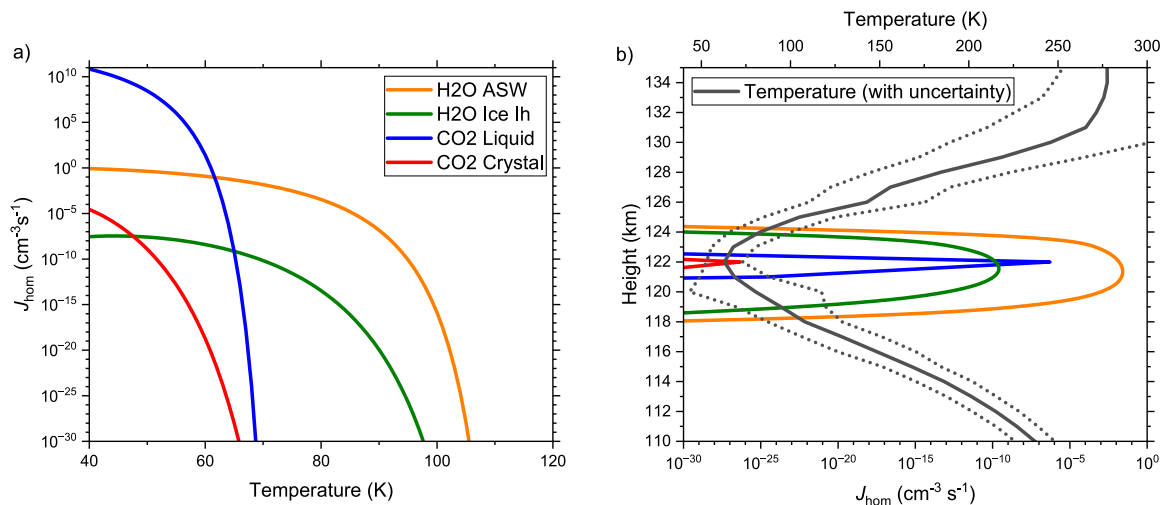
Figure 2. Homogeneous nucleation rates in the atmosphere of Venus. Panel (a) shows J_{hom} for CO_2 and H_2O particles in both an amorphous/liquid and crystalline form for an altitude of 121.6 km, where the pressure was 2.51×10^{-3} Pa (from the average atmospheric profile for 80°–90° latitude AM (AM refers to the morning terminator) in Mahieux et al. (2015)) and a mixing ratio of 1 ppm for H_2O and unity for CO_2. Panel (b) shows the corresponding J_{hom} values corresponding to the temperature and pressure profiles derived for Solar Occultation in the InfraRed profile 691.1, from the 12 March 2008 at 86.6° latitude from Mahieux et al. (2015).

2.1. Homogeneous Nucleation of CO_2 and H_2O Particles

Homogeneous nucleation directly from the vapor phase can occur under extreme conditions and it has been suggested that it may be important in the Earth's mesosphere (Lübken et al., 2009; Murray & Jensen, 2010). Given the conditions in the upper mesosphere of Venus are extremely cold, it is worth considering if H_2O or CO_2 particles might nucleate homogeneously. We have used a CNT formulation described by Määttänen et al. (2005). The equations and the choice of parameterizations of physical quantities are set out in Appendix A. Key physical quantities have been updated to be consistent with the latest experimental and theoretical studies. This includes the use of a parameterization of the vapor pressure of ASW from Nachbar et al. (2019), who showed that ASW is not simply the low temperature extension of supercooled liquid water and is in fact a distinct phase of water. We also derived a self-consistent interfacial energy for the liquid CO_2–vapor interface, based on measurements of homogeneous nucleation in a supersonic nozzle (Dingilian et al., 2020), and the ASW–vapor interfacial energy from studies of water uptake onto trapped nano-scale meteoric smoke analogs (Duft et al., 2019) (note that by self-consistent we mean that the interfacial energy is derived using the CNT and physical constant chosen in this paper, and then these CNT models are extrapolated to the conditions on Venus).

Nucleation rates (events per unit volume per unit time) for crystalline and amorphous/liquid-like phases of H_2O and CO_2 are shown in Figure 2a for an altitude of 121.6 km and a total pressure of 2.52×10^{-3} Pa (taken from the mean profiles derived from SOIR data in Mahieux et al. (2015)). We assumed a water mixing ratio of 1 ppm and the CO_2 mixing ratio was taken as unity (in practice it is around 0.96). In Figure 2b, we also show the homogeneous nucleation rate (J_{hom}, cm^{-3} s^{-1}) for one of the coldest temperature profiles in the SOIR data set, 691.1 from the 12 March 2008 at 86.6° latitude from Mahieux et al. (2015), where the temperature minimum was 63 ± 10 K at 122 km.

As expected, homogeneous nucleation of crystalline H_2O and CO_2 are very slow. In contrast, the homogeneous nucleation of ASW and liquid-like CO_2 might contribute to cloud particle populations. The nucleation rate for ASW is appreciable in this region and is relatively insensitive to temperature with values of around 10^{-2} cm^{-3} s^{-1} at 63 K, which would produce ~1 cloud particle per cm^3 in 100 s. While there are uncertainties in the physical constants that go into the calculation of J_{hom}, J_{hom} in this "plateau regime" has relatively weak temperature dependence (Figure 2a) and is therefore insensitive to those uncertainties. Since the plateau value of J_{hom} is defined by the rate of formation of ASW clusters, which in turn is related to the H_2O monomer concentration, this limit should be well defined and it is unlikely that the true J_{hom} of ASW is many orders of magnitude larger (or smaller). The same cannot be said for J_{hom} for liquid CO_2 at around 120 km in the atmosphere of Venus. J_{hom} for liquid CO_2 has a very strong temperature dependence above ~60 K; hence, uncertainties in temperature and various physical quantities can have a substantial effect on the nucleation rate. For example, while J_{hom} is relatively

small at 63 K, peaking at 10^{-5} cm^{-3} s^{-1} (Figure 2b), a shift of only 3 K to lower temperatures would increase J_{hom} to ~1 cm^{-3} s^{-1}. This would produce 100 particles per cubic centimeter in 100 s. Similarly, an interfacial energy only 15% smaller would also increase J_{hom} by more than five orders of magnitude. On this basis one should certainly not rule out the homogeneous nucleation of liquid CO_2 particles, which would then rapidly convert to crystalline CO_2 ice.

To summarize, the role of homogeneous nucleation in clouds at around 120 km in the atmosphere of Venus, we can state that nucleation of crystalline particles cannot occur, whereas homogeneous nucleation of ASW and liquid CO_2 is feasible. The resulting CO_2 particles would likely rapidly crystallize, as was observed in experiments (Dingilian et al., 2020), whereas ASW would likely persist in an amorphous state (Mangan et al., 2021). The nucleation of ASW would proceed at a rate of up to 10^{-2} to 10^{-3} cm^{-3} s^{-1} in layers of ~4 km wide depending on the shape of the temperature profile, whereas the nucleation of CO_2 might produce very high number concentrations in very narrow layers at the locus of the temperature minimum owing to the very strong temperature dependence of J_{hom}.

2.2. Heterogeneous Nucleation of CO_2 and H_2O Particles

For mesospheric water ice clouds on Earth and Mars, the primary INPs are thought to be MSPs (Hervig et al., 2021; Plane et al., 2018). In Venus' atmosphere, metals such as Fe, Mg, Si and Na are modeled to ablate from dust particles of mostly cometary origin within the altitude range shown in Figure 1 (Carrillo-Sánchez et al., 2020). The metal atoms become oxidized and then polymerize into MSPs (Plane et al., 2018). To the best of our knowledge, no other particle sources are available above 100 km in Venus' atmosphere. Hence, MSPs are a likely candidate for the nucleation of both CO_2 and H_2O particles.

The CNT formulation we adopt here has been used previously to evaluate the nucleation of CO_2 and H_2O in Mars' upper atmosphere (Listowski et al., 2013, 2014; Määttänen et al., 2005, 2007; Mangan, Salzmann, et al., 2017; Nachbar et al., 2016), but here we have updated the physical constants (see Appendix A). For CO_2 we use CNT to model the nucleation of crystalline ice on iron oxide or silica MSPs, and also on water ice. In addition, we used the KNT approach to study the nucleation of CO_2 on metal carbonates, which are a more likely composition of MSPs in the CO_2 atmosphere of Venus (Plane et al., 2018). Since the KNT approach is somewhat different from CNT, we introduce it separately in Section 2.4. Note that in the Venus' atmosphere, these metallic carbonates and oxides may be partially converted to metal chlorides by the large concentrations of HCl present (Mahieux et al., 2015). However, electronic structure theory calculations of the kind described in Section 2.4 show that polar metal chlorides would be even more effective nuclei for CO_2 and H_2O, if they form. Figure 3a shows the probability of nucleation in 1 second as a function of temperature for the four potential nucleation pathways based on CNT. Three of these pathways involve MSPs (0.4 nm radius): nucleation of ice I_h is defined by the experiments of Saunders et al. (2010) who quantified ice nucleation on MSP analogs in a cloud chamber at temperatures down to 180 K, reporting $m = 0.985$ at 190 K ($\theta = 10°$); nucleation of ASW on MSPs is defined by the experiments of Duft et al. (2019) who studied absorption and particle growth kinetics between 128 and 147 K, showing ASW was indeed the phase to nucleate under these conditions and surface adsorption of water resulting in an m of ~1; and nucleation of CO_2 on MSPs composed of iron oxides or silica was defined by Nachbar et al. (2016) between 64 and 73 K, reporting $m = 0.78 \pm 0.02$. In addition, we illustrate the nucleation of CO_2 on H_2O ice particles of 1 and 5 nm radius, where nucleation was defined experimentally by Glandorf et al. (2002) between 130 and 140 K, finding $m = 0.95$. Details of each of these CNT formulations are given in Appendix A.

Inspection of the nucleation probabilities in Figure 3a shows that the nucleation of ASW on 0.4 nm MSPs is most favorable, with nucleation probability increasing from an infinitely small value to unity on decreasing the temperature by only a few degrees. This occurs at a saturation ratio with respect to ASW of ~250, and larger MSPs would be expected to nucleate at even lower supersaturations. Nucleation probability of unity means that 100% of 0.4 nm MSP particles would activate to create ASW particles, hence consuming all MSPs before CO_2 or ice I_h might nucleate on them. If the MSP particle concentrations were 100 cm^{-3}, then a cloud of 100 ASW particles would nucleate and grow. These particles would only grow to a few nanometers given the availability of H_2O in the rarefied upper atmosphere of Venus. If the atmosphere were to become sufficiently cold, the curves in Figure 3a suggest that CO_2 might then nucleate on these small ASW particles. CO_2 is much more abundant than H_2O, and these particles would then grow rapidly (this is explored in more detail in Section 3 below).
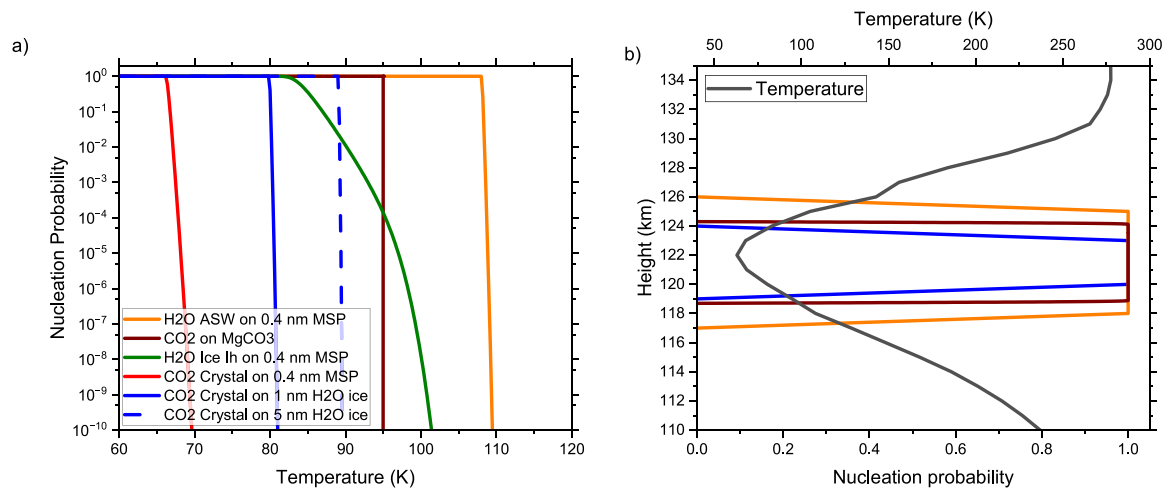
Figure 3. Probability of heterogeneous nucleation in the atmosphere of Venus. The nucleation probability is defined as the fraction of particles of defined size that nucleate ice in 1 second. (a) The probability, from our Classical Nucleation Theory formulation, of H_2O or CO_2 nucleating on Meteoric Smoke Particles (MSPs) (0.4 nm radius) or H_2O ice particles (1 and 5 nm radius) as a function of temperature, as well as the onset of particle growth from the Kinetic Nucleation Theory (KNT) model of CO_2 on $MgCO_3$ MSPs. These values correspond to an altitude of 121.6 km where the pressure was 2.51×10^{-3} Pa (from the average atmospheric profile for 80°–90° latitude morning terminator in Mahieux et al. (2015)) and a mixing ratio of 1 ppm for H_2O and unity for CO_2. (b) The nucleation probability corresponding to the temperature and pressure profiles derived for Solar Occultation in the InfraRed profile 691.1, from the 12 March 2008 at 86.6° latitude from Mahieux et al. (2015). We show the nucleation probabilities according to two potential mechanisms of CO_2 ice particle formation: first, is the direct nucleation of CO_2 on MSP according to KNT (Section 2.4), and second, the nucleation of amorphous solid water on MSP followed by the nucleation of CO_2 on H_2O ice (Section 2.1 and 2.2).

We examined heterogeneous nucleation corresponding to a specific SOIR profile (691.1) in Figure 3b. The probability of nucleation in 1 second is shown for the nucleation of ASW on MSP and for CO_2 on ice. We do not show the probability of nucleation of ice I_h or CO_2 on MSP because according to these calculations, all the MSP would be activated to form ASW particles long before the saturation was high enough for these other pathways to become active. It can be seen in Figure 3b that a broad layer of nanoscale ASW particles will form between 118 and 125 km. The ASW saturation point is around 120 K at 122 km, hence these ASW particles will persist until the temperature goes above this threshold or when they slowly sediment out of the layer. SOIR profile 691.1 is a particularly cold profile and under these conditions nucleation of CO_2 on ASW particles is favorable between 120 and 123 km. The nucleation of CO_2 on ice will occur at temperatures below 80 K for 1 nm particles and below 89 K for 5 nm particles (Figure 3a), but in an increasingly narrow layer when the temperature minimum is less deep. The prediction of CO_2 nucleation on ice is particularly sensitive to the uncertainties in the SOIR temperature retrievals. The quoted uncertainty at the temperature minimum is 10 K, which implies a range of likely values between 153 and 173 K. Even with the upper end of this range, the nucleation of crystalline CO_2 on amorphous ice is possible, albeit in a narrower layer of the atmosphere.

In summary, heterogeneous nucleation of ASW on MSPs is an effective pathway of producing water ice cloud particles in the upper atmosphere of Venus according to the parameterization defined by the experiments of Duft et al. (2019). However, due to the limited availability of water vapor, these ASW particles will remain less than around 5 nm in radius, but fill a layer ∼5 km thick. The number of heterogeneously nucleating ASW particles will be limited by the concentration of MSPs, but homogeneous nucleation of ASW may provide additional particles (we explore this in Section 2.3). If the temperature then decreases sufficiently, CO_2 will nucleate on these nanoscale ASW particles at a temperature dependent on their size. These CO_2 particles have the potential to grow rapidly and this will be explored in Section 3.

2.3. Competition Between Homogeneous and Heterogeneous Nucleation of ASW

We have shown that both homogenous and heterogeneous nucleation of ASW particles is feasible in the upper atmosphere of Venus. Now we examine which of these two mechanisms is likely to be more important in producing ice particles. In Figure 4, we show the number concentration of ASW particles resulting from both homogeneous and heterogeneous nucleation after 1 hr of constant conditions defined by SOIR profile 691.1. The number that nucleates heterogeneously is defined by the concentration of available MSP particles which we have set at
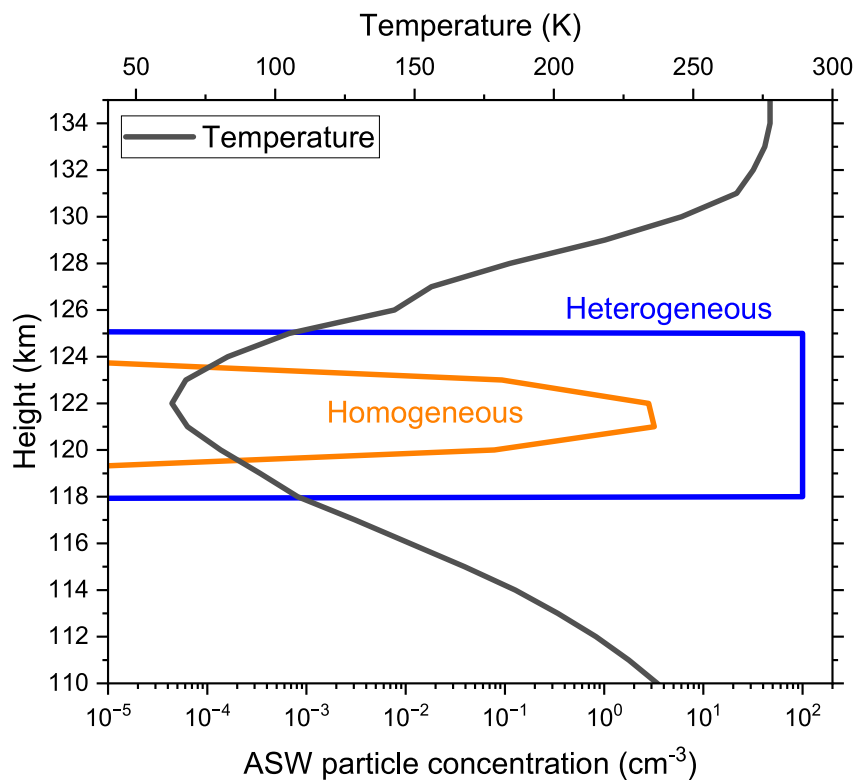
Figure 4. The competition between homogeneous and heterogeneous nucleation of amorphous solid water particles assuming conditions remain constant for 1 hr. The number concentration resulting from heterogeneous nucleation is defined by the product of probability of nucleation and the number concentration of Meteoric Smoke Particle particles of 0.4 nm (which we assume is 100 cm^{-3}). The temperature and pressure profile correspond to Solar Occultation in the InfraRed profile 691.1.

100 cm^{-3} here. This number is insensitive to time, since for most of the cloud layer the probability of nucleation is unity for a 1 s interval. In contrast, the number concentration of particles that nucleate homogeneously increases in proportion with time. For SOIR profile 691.1, homogeneous nucleation produces around 3 cm^{-3} ASW particles in 1 hr, whereas heterogeneous nucleation produces far more (depending on the assumed MSP concentration). If the cold pocket persisted for a day, one would expect (3 cm$^{-3} \times 24$) 72 cm^{-3} ASW particles over the course of the day. Sedimentation would then deplete the concentration, but there would be a persistent ASW production until the growth of ASW particles depleted the water partial pressure. In addition, it might be expected that cloud formation and sedimentation might deplete the MSP particle population, making homogeneous nucleation relatively more important. Another consideration is that the lifetime of the cold pocket is unclear and the high lapse rates associated with cold pockets may allow convection which would limit the time that homogeneous nucleation would be active for (but even a transient cold pocket would be enough to trigger homogeneous nucleation). Given the uncertainties in the rate of homogenous nucleation and temperature retrievals in Venus' atmosphere as well as the MSP concentration, we cannot rule out homogeneous nucleation as making a substantial contribution to the ASW particle population; however, if MSP are present, then the calculations indicate that heterogeneous nucleation will produce the majority of ASW particles in the upper atmosphere of Venus.

2.4. CO$_2$ Particle Formation on Carbonate MSPs From Kinetic Nucleation Theory

In Section 2.2 we established that a plausible mechanism for the formation of CO$_2$ ice particles is via the nucleation of ASW and the subsequent nucleation of CO$_2$ on those nanoscale ASW particles. Here we further explore the direct formation of CO$_2$ ice on MSP. In Figure 3a we showed, based on the data of Nachbar et al. (2016), that nucleation on MSP composed of iron oxides and silica occurred 40 K lower than ASW on MSPs, hence is unlikely to be an important process. However, in a CO$_2$ rich atmosphere like that of Venus we expect MSPs to be composed of metal carbonates rather than oxides (Plane et al., 2018), and hence we need to consider the nucleation of CO$_2$ ice on metal carbonates. We were not able to find the pertinent physical data for the wetting

properties of metal carbonate MSPs, so instead have used KNT. KNT is a bottom-up approach where the kinetics of adsorption and desorption of molecules to a cluster are treated explicitly (Bromley et al., 2016).

In these calculations, the INP were assumed to be $MgCO_3$ and $FeCO_3$ which have already been discussed as likely MSP building blocks in the analogous atmosphere of Mars (Plane et al., 2018). The size of these seed particles was fixed at a radius of 0.35 nm, corresponding to a single $MgCO_3$ molecule with three CO_2 molecules bound to it (Plane et al., 2018). Because of the very large dipole moment of $MgCO_3$ ($\mu_D = 11.6$ Debye), these CO_2 molecules are strongly bound enough for the $MgCO_3(CO_2)_3$ complex to be stable at temperatures below 150 K (Plane et al., 2018). Rate coefficients for the addition of subsequent CO_2 molecules up to $MgCO_3(CO_2)_{40}$ were then calculated using Rice Ramsperger Kassel Markus (RRKM) theory (Gilbert & Smith, 1990) with a solution of the Master Equation based on the inverse Laplace transform method (De Avillez Pereira et al., 1997). Electronic structure theory calculations (Frisch et al., 2016) were used to compute the vibrational frequencies of the small clusters up to $n = 4$. See Appendix B for details of these calculations and the derivation of the uptake coefficient, γ, for CO_2 attachment to an $MgCO_3(CO_2)_n$ cluster, and the rate of evaporation of the new cluster (i.e., $MgCO_3(CO_2)_{n+1} \rightarrow MgCO_3(CO_2)_n + CO_2$). Although γCO_2 is estimated to approach unity for cluster sizes larger than $n = 15$ at temperatures below 150 K (Figure B1a), we limit the value here to $\gamma CO_2 \leq 0.1$ to allow for the high pressure limiting attachment rate of CO_2 for $MgCO_3(CO_2)_n$ to be lower than the hard sphere collision frequency (Smith, 1980). γCO_2 and the evaporation rate were computed at a pressure of 1.33×10^{-3} Pa (10^{-5} Torr), which is the typical pressure at ~150 km in Venus' atmosphere (Mahieux et al., 2015). γCO_2 at a lower altitude was then scaled by the relative atmospheric density up to the limit of 0.1. The evaporation rate was then computed using detailed balance with the CO_2 attachment rate, with an equilibrium constant calculated using statistical mechanics with the partition functions for $MgCO_3(CO_2)_{n+1}$ and $MgCO_3(CO_2)_n$ using the vibrational frequencies and rotational constants described in Appendix B. For clusters larger than $n = 40$, γCO_2 was set to 0.1 at all temperatures below 180 K, and the equilibrium constant (and hence the evaporation rate) was estimated from the Antoine relation for gas-phase CO_2 above the solid (Chicko, 2022; Giauque & Egan, 1937).

The conditions under which CO_2 particle growth becomes favorable are indicated in Figure 3. MSPs can provide a site where a CO_2 cluster is stabilized leading to the growth of CO_2 particles at temperatures below about 95 K at 122 km. The initial cluster is non-crystalline but on subsequent growth this material is likely to deposit as crystalline CO_2. However, if heterogeneous nucleation of ASW particles is as effective as indicated by our CNT formulation and the study of Duft et al. (2019), then the majority of MSP particles would have already activated to form nanoscale ASW particles. On the other hand, if the atmosphere were dehydrated by a previous cloud event, then new MSP particles might nucleate CO_2 in preference to ASW. Nevertheless, the most likely route to CO_2 particles is the nucleation of CO_2 on ASW particles.

2.5. Planetary Wide Viability of H_2O and CO_2 Ice Particle Formation

In order to assess the geographical distribution and occurrence frequency of cloud formation conditions, we have plotted the SOIR profiles from Mahieux et al. (2015), broken down into latitude bands and morning or evening terminator, in Figure 5. The SOIR temperature profiles are then compared to the threshold temperatures at which ASW and crystalline CO_2 become saturated (the phases that are expected to make up clouds) as well as the temperature at which the nucleation rate of ASW on 1.0 nm ASW particles and CO_2 on 5 nm ASW particles is equal to 1 s^{-1} (equivalent to a nucleation probability in 1 s of 0.63).

While there is considerable variability of the temperature profiles, many of the profiles exhibit a minimum around 120–130 km with a value below the temperature required for the nucleation and persistence of both ASW and CO_2 ice particles (see Figures 5 and 6). There is also a substantial uncertainty in the retrieved temperatures, which is generally greatest at the temperature minimum (and also increases dramatically above ~150 km; see Figure 1.). The quoted temperature uncertainty typically ranges from 10 to 40 K at a temperature minimum between 115 and 130 km. Even considering this uncertainty many profiles have a sufficiently low temperature to allow the nucleation of both ASW and CO_2 crystals. In the following, we quote estimates of the frequency with which nucleation will occur based on the best estimate of temperature from Mahieux et al. (2015). We also note that a more recent analysis of the SOIR data set by Mahieux et al. (2023) suggests that the average temperature in the upper mesosphere is higher than those reported by Mahieux et al. (2015), although minima well below 100 K are still reported. This illustrates the difficulty of retrieving or measuring the temperature of the upper mesosphere of Venus.
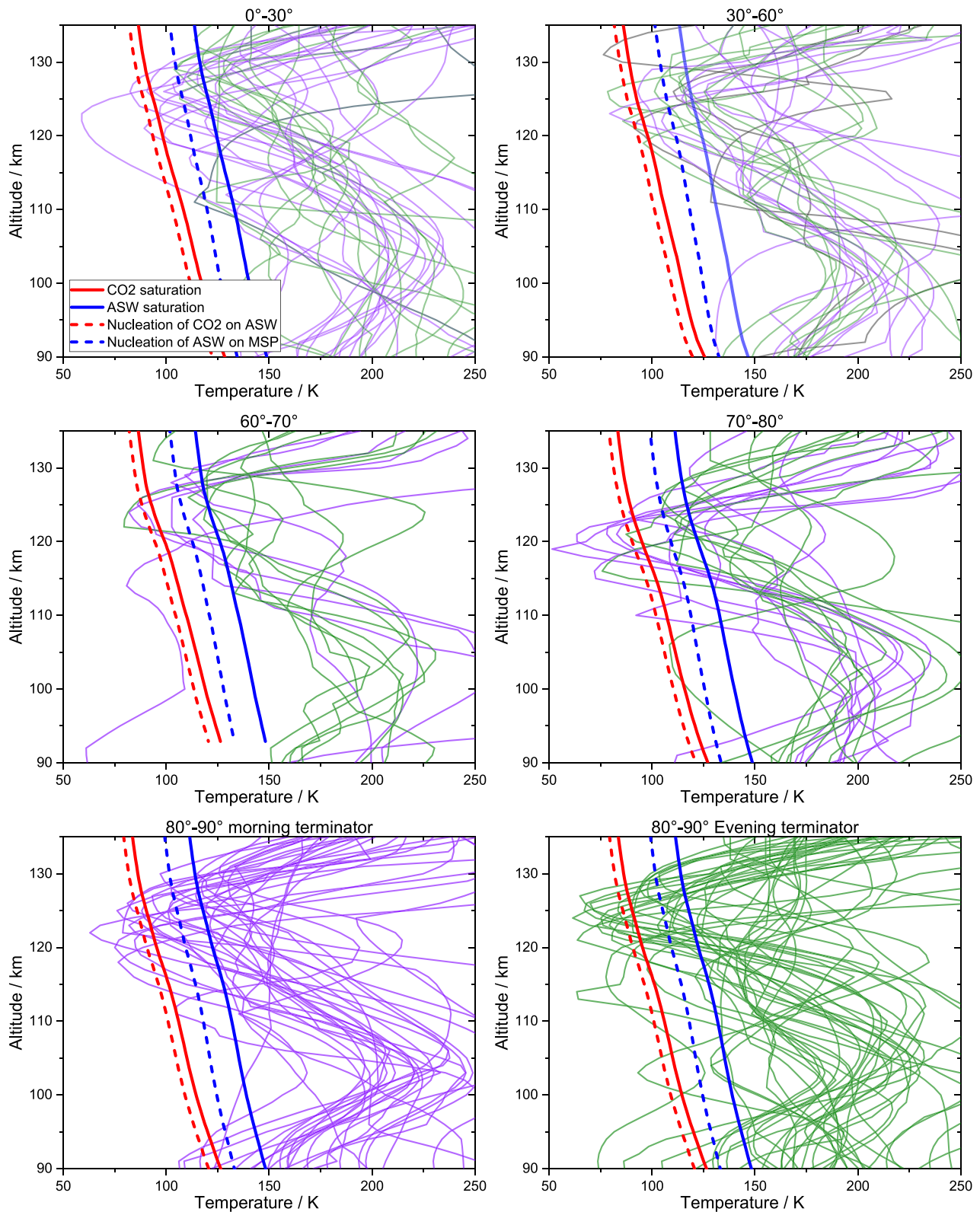
Figure 5. Latitude (0°–90°) and time of day dependence (morning terminator in purple or evening terminator in green) of saturation point temperature for crystalline CO_2 and amorphous solid water (ASW) and of the nucleation activation temperatures (where $J_{het} = 1 \text{ s}^{-1}$, corresponding to a nucleation probability of 0.63 in 1 s; we show values for nucleation of ASW on 1.0 nm Meteoric Smoke Particle particles and CO_2 on 5 nm ASW particles). We do not explore seasonal dependence since the Venus day takes about half of a Venus year. Temperature profiles are taken from Mahieux et al. (2015) and the mean morning terminator pressure profiles from the same paper are used to derive the saturation and the nucleation activation temperatures.
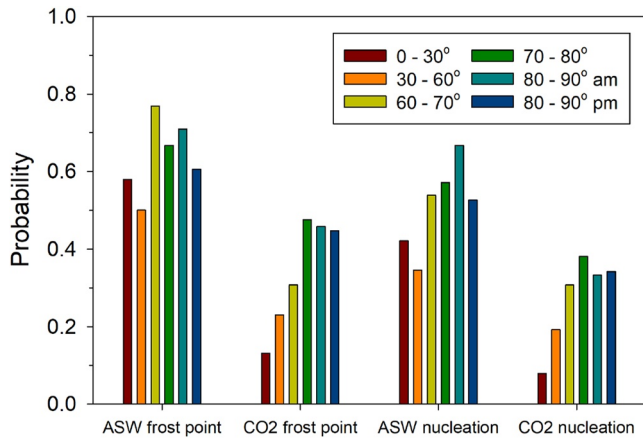
Figure 6. Probability of atmospheric temperature falling below the H_2O and CO_2 frost points, and that required by Classical Nucleation Theory for particle nucleation above 100 km, using the observed temperature profiles from the data set of Mahieux et al. (2015). The probability is defined as the fraction of individual Solar Occultation in the InfraRed (SOIR) profiles where the temperature dropped below the respective frost point or nucleation threshold (see Figure 5). These probabilities are cumulative, meaning that when the SOIR temperature profile is below the CO_2 frost point, for example, the atmosphere is also supersaturated with respect to amorphous solid water.

On average across all latitudes, 64% of the profiles indicate that the atmosphere is supersaturated with respect to ASW in a layer ∼5–10 km deep. The nucleation of ASW on MSPs is also possible in 51% of the profiles on average. The sedimentation velocity of a 5 nm ASW particle at 120 km is 0.7 m s^{-1}; hence, these particles would form a layer 5–10 km thick and have a lifetime with respect to sedimentation on the order of hours. This indicates that clouds composed of nanoscale ASW particles should be a regular feature of the atmosphere of Venus at around 120 km at all latitudes. This conclusion holds when we consider the reanalyzed SOIR temperature profiles from Mahieux et al. (2023), albeit the frequency of occurrence of ASW clouds would be lower.

Nucleation of CO_2 on ASW particles is also remarkably frequent, occurring in 27% of the profiles on average. The frequency of CO_2 nucleation has latitude dependence, with ∼30%–40% of profiles between 60° and 90° dipping below the threshold required for the nucleation of CO_2 on 5 nm ASW particles. Even at low latitudes (0–30°), ∼8% of profiles were sufficiently cold for nucleation of CO_2 on ASW. Hence, CO_2 cloud formation is also relatively frequent at all latitudes. If we instead consider the temperature profiles reported by Mahieux et al. (2023), then a smaller subset of profiles becomes supersaturated with respect to ice and the occurrence of CO_2 Venusian mesospheric clouds (VMCs) would be expected to be lower. Given the uncertainty in the temperature retrievals in Venus' upper mesosphere, we conclude that VMCs composed of nanoscale ASW particles will be common, but the presence of CO_2 ice clouds is highly uncertain. Hence, efforts to observe CO_2 VMCs would help constrain the temperature of Venus' upper mesosphere. We now turn our attention to the properties and lifetime of CO_2 VMCs and if they should be observable with contemporary satellite instruments.

3. Modeling Ice Particle Evolution in Venus' Upper Atmosphere

In order to explore the evolution of the CO_2-ice clouds (the VMCs), a 1-dimensional model was constructed which describes the nucleation, growth, sedimentation and sublimation of the ice particles. The model is described in Appendix C. The model is initiated with vertical profiles of atmospheric density and temperature determined using the SOIR instrument (Mahieux et al., 2015) that had a deep temperature minimum (<90 K) so that CO_2 would have been highly supersaturated and coagulation is neglected since the lifetime of these clouds is relatively short. Figure 3 shows that under these conditions, nucleation of CO_2 ice particles occurs either directly on MSPs or on ASW particles that had earlier nucleated on MSPs. Since the concentration of ASW particles depends on the concentration of MSP particles both pathways to formation of CO_2 ice particles would produce similar VMCs. Hence, our 1-D microphysical model produces CO_2 ice crystals through the direct nucleation on MSP, but the results would be similar for the case where CO_2 nucleates on ASW particles. Once CO_2 particles are nucleated, the model follows the fate of the particles as they grow, sediment and finally sublimate on entering a warmer region.

Figure 7 shows examples of model output, corresponding to two examples of cloud that can be produced from the observed SOIR temperature profiles. The first example peaks around 120 km with particles around 100–200 nm radius, and the second persists for longer and peaks around 110 km with particles that can exceed 2 μm in radius. The first cloud category is produced by deep but relatively sharp temperature minima above 120 km (e.g., orbit 671.1). In contrast, the much larger particles in the second cloud category are produced by much broader temperature minima, in this case between ∼112 and 122 km (e.g., orbit 1,581.1). Figure 7b shows the time evolution of the particle size and height for these two examples. The first cloud only lasts for ∼350 s, and the second type lasts for around 1,200 s (20 min). The latter example is the most pronounced cloud that was generated in the model from the SOIR data set (orbit 1,581.1 at 87.3° on the 19 August 2010) but is still relatively short-lived because sedimentation is so rapid in this altitude range. Figure 8 also illustrates a composite of clouds predicted for multiple SOIR profiles at 70–80° and 80–90° bands (north and south), showing that these clouds all have similar features, with small CO_2 particles at higher altitudes that rapidly grow and sediment until they sublime 5–10 km
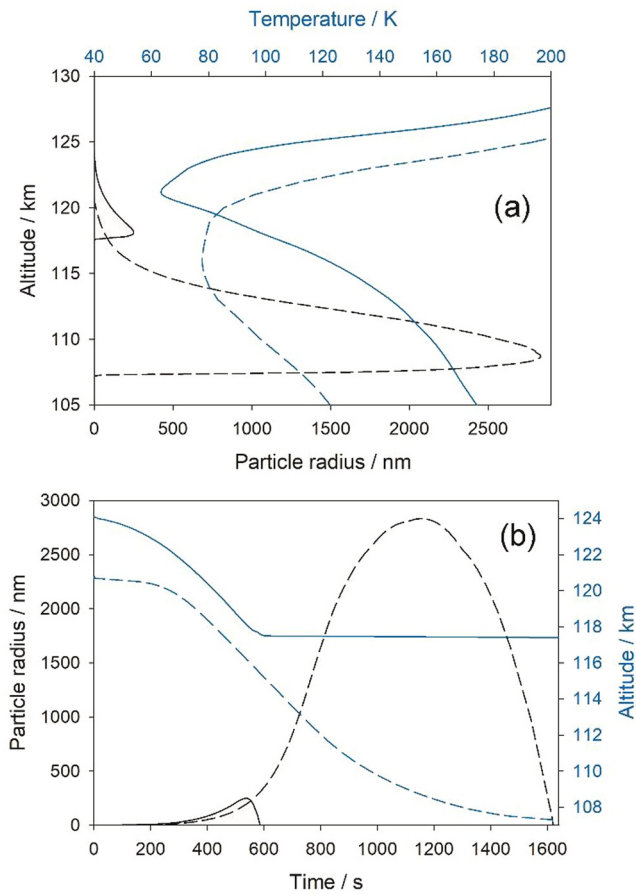
Figure 7. The microphysics of CO_2 ice clouds (a) Modeled CO_2 particle nucleation, growth, sedimentation, and sublimation for the temperature profile of orbit 671.1 at 82.9° (solid lines), and orbit 1,581.1 at 87.3° (dashed lines). (b) Time evolution of the radius and height of the CO_2 particles ($\gamma CO_2 = 0.1$, Meteoric Smoke Particle concentration = 100 cm^{-3}).

below the cold point. Note that the depth of clouds at 80–90° is generally greater than that at 70–80°, as a result of the broader temperature minimum at higher latitudes.

4. Detectability of VMC Ice Clouds

We have shown that conditions are likely to exist in the upper mesosphere of Venus where both ASW and CO_2 ice clouds can form. Scattering by nanoscale ASW particles will not be observable; however, if CO_2 ice crystals form, we have shown that they could reach sizes of 100s nm to micron sizes. Hence, we now address the question of whether these VMCs should be observable. The best chance of detection is likely through satellite observations of optical extinction. In this section, we evaluate the possibility of detecting these high-altitude clouds in existing data sets by calculating the extinction by CO_2 ice particles using Mie theory. Venus Express had a suite of three instruments onboard that profiled cloud and haze layers at lower altitudes on Venus. The first two are the UV and near-IR channels of the SPICAV instrument (Spectroscopy for the Investigation of the Characteristics of the Atmosphere of Venus) (although we do not include the near-IR channel in our current analysis). The UV channel has a wavelength range of 118–320 nm, and it performs stellar and solar occultations in addition to nadir and limb observations. The third instrument is SOIR which measures across the near- to mid-IR from 2.2 to 4.3 μm (or 2,200–4,400 cm^{-1}) in solar occultation only. SPICAV has provided observations of the cloud and haze layers of Venus (Luginin et al., 2016; Wilquet et al., 2009, 2012), and SOIR observations were used also by Wilquet et al. (2009, 2012) and Takagi et al. (2019) who observed an increase in aerosol mixing ratio above 100 km, whereas the other studies reported results on clouds and hazes only at altitudes below 100 km. For the purposes of our Mie calculations, we selected the wavelength at 220 nm for SPICAV-UV and at 3,320 nm for SOIR; both instruments have a similar detection limit around 1×10^{-5} km^{-1} (Wilquet et al., 2009).

We evaluate the detection probability of H_2O core (1 nm radius) CO_2 shell particles that might form at an altitude of 120 km by determining the Mie extinction cross sections of individual particles as a function of radius. We use refractive indices for CO_2 from the literature (Hansen, 1997, 2005; Warren, 1986), and those for water ice at 220 and 3,320 nm from Kofman et al. (2019) and Warren and Brandt (2008), respectively. At 220 nm the water ice refractive indices were measured specifically for low density amorphous ice at 70 K (Kofman et al., 2019).

In Figure 9, we show the extinction for CO_2 particles at varying radii and particle concentrations. Figure 7 shows that CO_2 particles often grow into the 100s nm range, hence extinction above the detection limit at both 220 and 3,320 nm is possible with a sufficiently high number concentration. However, at 220 nm extinction exceeds the detection limit for much smaller particles and lower number concentrations. For example, for CO_2 ice particle concentration of 100 cm^{-3}, detection at 220 nm using SPICAV-UV would occur when the particles were larger than ~25 nm, whereas for detection at 3,320 nm with SOIR, the particles would need to be above ~160 nm.

We now evaluate the detectability at 220 nm of the clouds modeled in the previous section and the sensitivity of the results to the CO_2 uptake coefficient (γCO_2) and the MSP particle concentration. In the previous section γCO_2 was set equal to 0.1. Figure 10a illustrates the sensitivity of the cloud formation to γCO_2, for the atmospheric temperature/density profile from orbit 671.1 used previously, and with the MSP particle concentration fixed at 100 cm^{-3} between 110 and 130 km. As expected, the peak particle size varies with γCO_2, for example, when γCO_2 is decreased by a factor of 100 from 0.1 to 10^{-3} the peak particle size only decreases by a factor of ~10, and the peak height is essentially unchanged. This variation has consequences on the detectability of the particles. Figure 10b shows the optical extinction at 220 nm of the cloud as a function of γCO_2 for the same atmospheric
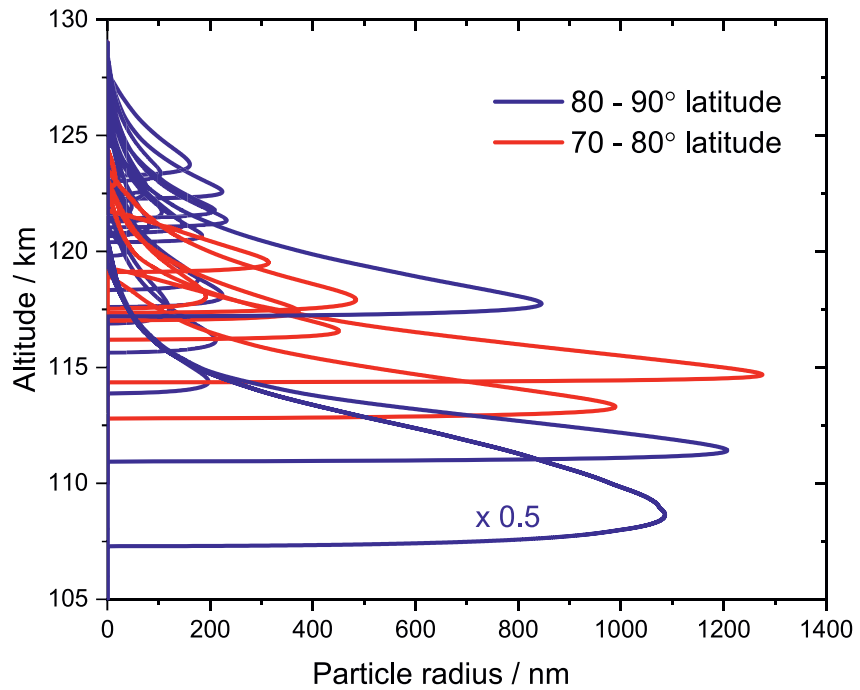
Figure 8. Modeled particle nucleation, growth, and sedimentation of CO_2 particles initiated with multiple observed temperature profiles from the data set of Mahieux et al. (2015) using $\gamma CO_2 = 0.1$ at two latitude ranges.

profile. The Mie extinction is a strong function of particle size, and so this cloud would be barely detectable (for the SPICAV-UV detection limit of 10^{-5} km^{-1}) if γCO_2 was less than 0.005.

In addition to the particle size, particle concentration plays a role in the detectability of the clouds. In Figure 11, we test the sensitivity of the modeled cloud extinction to the assumed number of MSP particles, with γCO_2 fixed at 0.1. In this case, the cloud would not be detectable if the MSP number density fell below ~ 1 cm^{-3}. However, the MSP concentration is probably much higher than this because a similar quantity of metal atoms is predicted to be injected via meteoric ablation into the upper atmospheres of Venus and Earth (12.6 and 8.3 tonnes d^{-1},

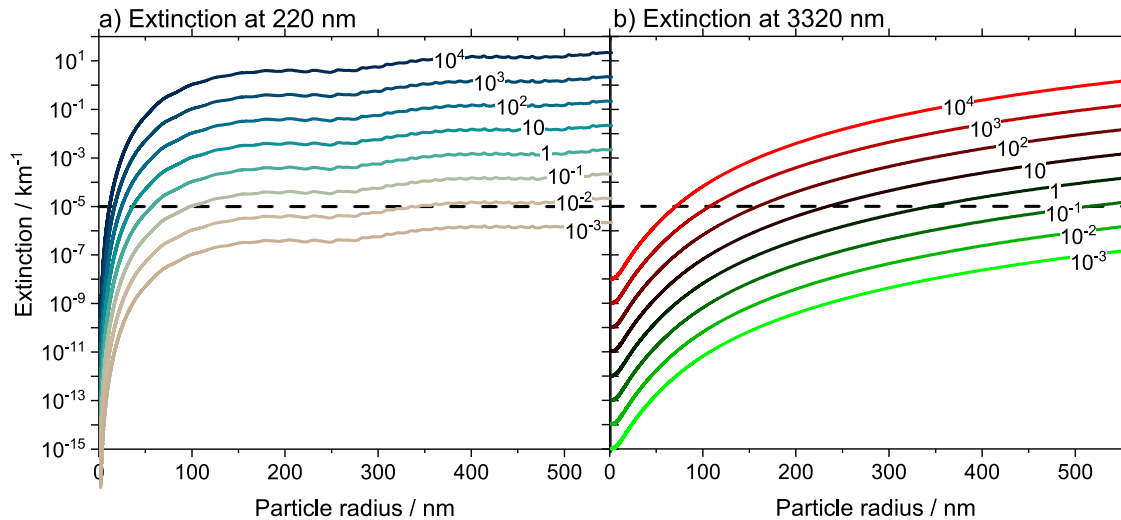**Figure 9.** Predicted extinction coefficients in km^{-1} for Venusian mesospheric clouds with particle radius for different particle concentrations (cm^{-3}) at (a) 220 and (b) 3,320 nm for CO_2 particles with 1 nm radius H_2O cores. The dotted line shows the detection limits 1×10^{-5} km^{-1} for SPICAV-UV and Solar Occultation in the InfraRed at 120 km. The particle concentrations (cm^{-3}) are indicated.
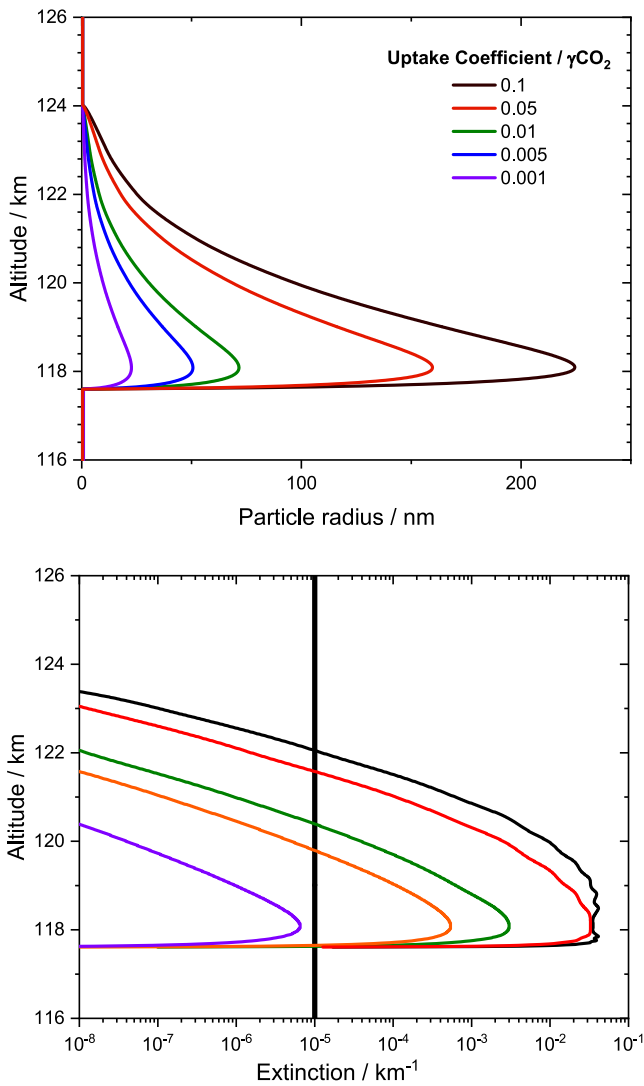
Figure 10. Sensitivity of (a) CO_2 ice particle growth and (b) optical extinction at $\lambda = 220$ nm, to the CO_2 uptake coefficient (γCO_2) for the conditions of orbit 671.1 (82.9° latitude) from Mahieux et al. (2015). Number density of Meteoric Smoke Particle particles = 100 cm^{-3}. The gray line in panel (b) shows the detection limit (1×10^{-5} km^{-1}) of the Solar Occultation in the InfraRed instrument onboard Venus Express.

respectively), and the MSP concentration in the terrestrial mesosphere above 75 km is around 2,000 cm^{-3}, based on rocket-borne charge particle measurements and modeling (Plane et al., 2014).

These sensitivity studies show that even if either the concentration of MSPs or the uptake coefficient γCO_2 were a couple of orders of magnitude lower than for the standard model run, the resulting CO_2-ice clouds would still be detectable. However, it is their very short lifetime of only minutes, which would need to coincide with a satellite observation, will make the detection of these clouds challenging. The model results of Listowski et al. (2014) revealed similar short lifetimes for mesospheric CO_2 clouds on Mars that were dictated by the duration of the supersaturated cold pockets. They concluded that the scarcity of cloud observations among the hundreds of supersaturated temperature profiles observed by SPICAM was very probably due to the short lifetimes (<1–2 hr) of the cold pockets formed by upward propagating gravity waves, and of the clouds themselves that rapidly evaporate in subsaturated conditions (10–20 min) (Listowski et al., 2014). If the cold pockets on Venus are a result of similar gravity waves as on Mars, the cold pocket lifetime of 1–2 hr is a lower limit. According to our simulations (see Figure 8), this cold pocket duration is sufficiently long for a detectable cloud to form, sediment to a subsaturated environment and evaporate (<20 min). Nevertheless, the satellite observation would need to happen exactly at the right time and in the right place to be able to catch these ephemeral clouds. Another possibility for satellite detection would be using limb observations rather than solar occultation. SPICAV UV limb observations have been used to study nightglow (Gérard et al., 2008), and IR limb observations have been used to study scattering layers below 90 km. UV limb scanning techniques could also perhaps be used to search for VMCs as they are done on Mars (Clancy et al., 2019).

5. Conclusions

The upper mesosphere of Venus between around 115 and 130 km is frequently cold enough that the atmosphere is supersaturated with respect to H_2O ice and possibly CO_2 ice. Based on a combination of classical and kinetic nucleation theory, we propose that there is a persistent ASW H_2O cloud layer on Venus around 10 km deep centered around 120 km. These ASW particles may form both from heterogeneous nucleation on MSPs or can form homogeneously directly from the vapor phase if the temperature minimum persist for more than a few hours. The ASW cloud particles are unlikely to grow substantially larger than ∼5 nm given the limited amount of water vapor present in the upper mesosphere of Venus. Hence, we suggest that there is a persistent sub-visible layer of water ice particles composed of ASW which could cover as much as 50% of Venus at all latitudes, but this fraction is sensitive to uncertainties in the retrieved temperature. This 50% value is also derived assuming that the terminator pressure and temperature measurements from SOIR are representative of other times of the Venus day. Nevertheless, the presence of clouds of nanoscale ASW particles in the upper mesosphere is highly likely.

We also present evidence that CO_2 ice crystals may nucleate on either ASW particles or even on bare MSPs. At latitudes greater than 60° (N and S), nucleation on ASW particles can occur in more than 30% of the SOIR profiles from Mahieux et al. (2015). However, there is substantial uncertainty in the retrieved temperatures and more recent analysis suggests the temperature of the upper mesosphere is several 10s of degrees warmer than in the 2015 analysis (Mahieux et al., 2023), which would substantially reduce the probability of CO_2 nucleation. Nevertheless, the nucleation of CO_2 ice particles cannot be ruled out given the uncertainties in the retrieved temperature. Since CO_2 is the primary component of Venus' atmosphere, CO_2 particles will grow rapidly to 100s
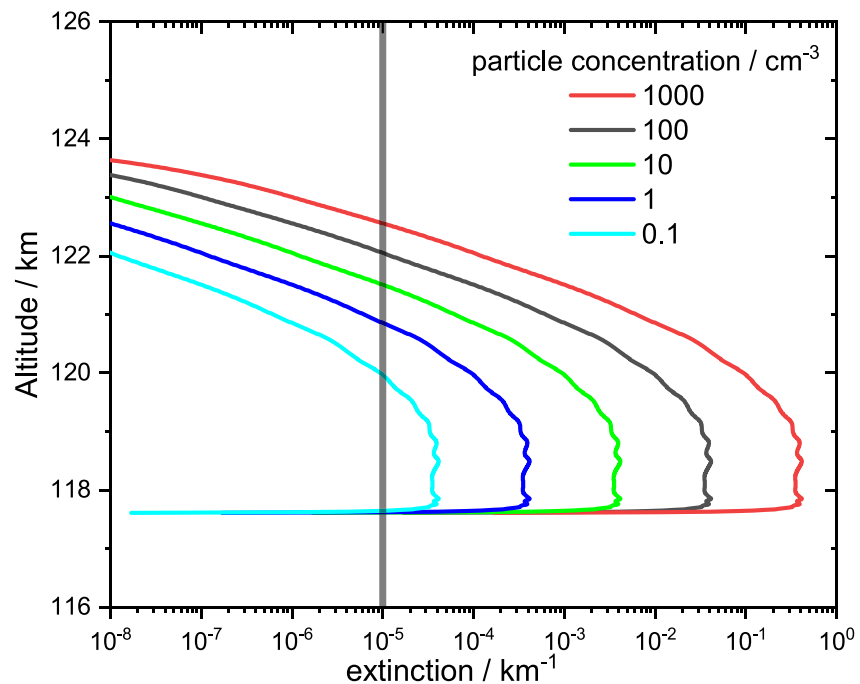
Figure 11. Extinction of CO_2 ice particles at $\lambda = 220$ nm for a range of Meteoric Smoke Particle concentrations for the conditions of orbit 671.1 ($\gamma CO_2 = 0.1$) from Mahieux et al. (2015). The gray line shows the estimated detection limit of the Solar Occultation in the InfraRed instrument onboard Venus Express.

nm in only minutes. However, these clouds will only have a lifetime of ~10–20 min since sedimentation is very rapid in the thin upper mesosphere of Venus. These CO_2 ice particles are most likely composed of crystalline CO_2 ice-I and will likely have a cubic, octahedral, or cubo-octahedral shape (Mangan, Salzmann, et al., 2017). These clouds may also produce halos that are unique to carbon dioxide crystals, as recently suggested for Mars (Ding et al., 2023). To an observer, VMCs might appear similar to *cirrus uncinus* (mares' tails) on Earth where nucleation occurs close to the temperature minimum, followed by sedimentation and growth and subsequent sublimation of the ice crystals as they fall into a subsaturated warmer region. Any wind shear would give the fall streaks curvature (*uncinus*), where falling ice crystals are blown laterally as they sediment.

We have explored whether VMCs might be observable with instruments on Venus Express. We find that the extinction will be large enough to observe at both 220 nm (SPICAV) and 3,320 nm (SOIR); however, the probability of an observation occurring in the 10–20 min that a cloud was present would be small. Nevertheless, we recommend that analysis of satellite data should be extended to altitudes where VMCs are predicted to occur, and that VMCs should be a target for future missions to Venus. Positive identification of CO_2 VMCs would help define the range of temperatures possible in the upper mesosphere of Venus.

Given the strong sedimentation of VMC particles, VMCs have the potential to redistribute material in the upper atmosphere of Venus. Since the nucleation of CO_2 on ASW with meteoric smoke cores is a likely mechanism for their production, VMCs are likely to transport MSPs to lower altitudes where they will be released in relatively narrow layers on the sublimation of CO_2 ice crystals (Figure 12). The formation of CO_2 crystals may also lead to the uptake of gas-phase meteoric species, which would also be released in a particulate form as the cloud particles sublimed at the base of the cloud layer (Mangan, Frankland, et al., 2017). Similarly, VMCs will redistribute water vapor downwards, although the efficiency with which VMCs serve as a "cold trap" will depend on the extent to which ASW particles can quench the supersaturation. On Earth, mesospheric clouds redistribute water downwards, resulting in a layer of enhanced water vapor at the base of the clouds, affecting odd oxygen and hydrogen chemistry (Murray & Plane, 2003, 2005). The extent to which VMCs limit the loss of water to space form Venus' atmosphere should be the subject of more detailed microphysical modeling constrained by observations.

Overall, this work reveals that there are clouds in the upper mesosphere of Venus around much of the planet, potentially involving both water and CO_2 ice particles. We predict a ubiquitous layer of nanoscale water ice
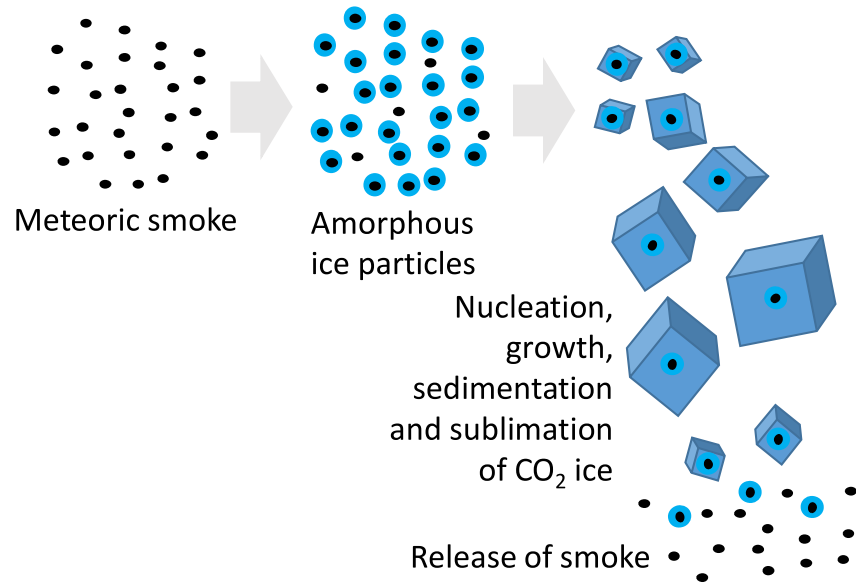
Figure 12. Formation and dissipation of Venusian mesospheric clouds. Meteoric Smoke Particles (MSPs) nucleate nanoscale amorphous ice particles, followed by the nucleation of CO_2 on those particles. The CO_2 crystals rapidly grow, probably with a cubic, octahedral or cubo-octahedral shape (Mangan, Salzmann, et al., 2017), then sediment and release the MSPs as they sublime in a warmer part of the atmosphere.

particles that forms both homogeneously and heterogeneously and then provides the substrate on which CO_2 VMC particles can nucleate if the temperature falls well below 100 K. The resulting crystals of CO_2 would grow rapidly to sizes where they can fleetingly scatter light at a detectable level before sedimenting into a warmer layer where they sublime.

Appendix A: Classical Nucleation Theory Formalism

In this section we describe the nucleation theory we have applied to the atmosphere of Venus for both nucleation of CO_2 and H_2O phases and give the pertinent parameters in Table A1.

Table A1
Physical Properties of H_2O and CO_2

Property	Value	Notes
ASW		
Saturation vapor pressure	$P_{sat,hex} \cdot \exp\left(\frac{2312 - 1.6T}{RT}\right)$	Nachbar et al. (2018)
Density	940 kg m^{-3}	Ghormley and Hochanadel (1971)
Surface tension	0.085 J m^{-2}	Derived from Duft et al. (2019)
Desorption energy on MSP	42 kJ mol^{-1}	Duft et al. (2019)
Vibrational frequency	10^{13} s^{-1}	Pruppacher and Klett (1997)
Mean jump distance	0.32 nm	Pruppacher and Klett (1997)
Contact parameter on MSP	0.999	Duft et al. (2019) suggest $m = 1$
Ice I$_h$		
Saturation vapor pressure	$\exp(9.550426 - 5{,}723.265/T + 3.53068 \ln(T) - 0.007728332T)$ (Pa)	Murphy and Koop (2005)
Density	$(-1.3103{\cdot}10^{-9}\,T^3 + 3.8109{\cdot}10^{-7}T^2 - 9.2592{\cdot}10^{-5}T + 0.94040) \cdot$ 1,000 (kg m^{-3})	Murray and Jensen (2010)
Surface tension	$0.141 - 0.00015T$ (J m^{-2})	Hale and Plummer (1974)

Table A1
Continued

Property	Value	Notes
Desorption energy	17.5 kJ mol^{-1}	Seki and Hasegawa ([1983])
Vibrational frequency	10^{13} s^{-1}	Määttänen et al. ([2005])
Mean jump distance	0.32 nm	Pruppacher and Klett ([1997])
Contact parameter on MSP	0.985	Saunders et al. ([2010])
CO_2 crystal		
Saturation vapor pressure	$1.38 \cdot 10^{12} \exp(-3182.48/T)$ (Pa)	Azreg-Aïnou ([2005])
Density	$1.72391 - 2.53 \cdot 10^{-4}T - 2.87 \cdot 10^{-6}T^2$ (g cm^{-3})	Mangan, Salzmann, et al. ([2017])
Surface tension	0.08 (J m^{-2})	Nachbar et al. ([2016]) and Wood ([1999])
Desorption energy	18.5 kJ mol^{-1}	Nachbar et al. ([2016])
Vibrational frequency	$2.9 \cdot 10^{12}$ s^{-1}	Nachbar et al. ([2016])
Mean jump distance	0.4 nm	Nachbar et al. ([2016]) and Wood ([1999])
Contact parameter on ice	0.95	Glandorf et al. ([2002])
Contact parameter on MSP	0.78	Nachbar et al. ([2016])
CO_2 liquid		
Saturation vapor pressure	$= 101{,}325 \cdot 10^{-A}$ $A = 1353/T - 8.143 \cdot \log(T) + 0.006259T + 24.619$	Dingilian et al. ([2020]) and Michels et al. ([1950])
Density	$\ln\left(\frac{\rho'}{\rho_c}\right) = \sum_{i=1}^{4} a_i \left(1 - \frac{T}{T_c}\right)^{t_i}$ $a_1 = 1.9245108;\ a_2 = -0.62385555;\ a_3 = -0.32731127;$ $a_4 = 0.39245142;\ t_1 = 0.34;\ t_2 = 0.5;\ t_3 = 10/6;\ t_4 = 11/6;$ $T_c = 304.1282$ K$;\ \rho_c = 467.6$ kg m^{-3}	Dingilian et al. ([2020]) and Span and Wagner ([1996])
Surface tension	0.0378 J m^{-2}	Derived from fit to data in Dingilian et al. ([2020]), see text

Note. Notes on the choice and derivation of physical properties of condensed phases of H_2O and CO_2.

A1. Homogeneous Nucleation

The CNT formulation we have chosen to use for homogeneous nucleation is based on the equations set out by Määttänen et al. ([2005]). The free energy of formation of a spherical cluster of molecules with a radius r is described by

$$\Delta F_{\text{hom}} = -\frac{4\pi r^3}{3v} kT \ln S + 4\pi r^2 \sigma \tag{A1}$$

where v is the molecular volume of the condensed phase, σ is the interfacial energy between the condensed phase and the vapor phase, k is the Boltzmann constant, T is the temperature, and S is the saturation ratio. A cluster is said to reach a critical size when the volume term (the left hand term) starts to dominate over the surface term (the right hand term). At the critical size, further growth by addition of monomer results in an increase in stability; hence, the critical cluster size and free energy of formation can be derived

$$r^* = \frac{2v\sigma}{kT \ln S} \quad \text{and} \quad \Delta F_{\text{hom}}^* = \frac{16\pi v^2 \sigma^3}{3(kT \ln S)^2} \tag{A2}$$

The homogeneous nucleation rate is defined by an Arrhenius-like expression

$$J_{\text{hom}} = f_{\delta T} Z_{\text{hom}} \beta_{\text{hom}} c_{1,v} \exp\left(\frac{-\Delta F_{\text{hom}}^*}{kT}\right) \tag{A3}$$

where $c_{1,v}$ is the concentration of monomers in the vapor phase. The dimensionless non-isothermal coefficient $f_{\delta T}$ as described in Feder et al. ([1966]) accounts for a reduction in the nucleation rate in cases when the atmospheric concentration of the nucleating species comprises a significant fraction of the total atmosphere. Higher

collision frequency with the nucleating species compared to the inert carrier gas means the heat of condensation is not efficiently removed from the cluster, leading to lower $f_{\delta T}$ values and therefore lower nucleation rates. In the case of water ice nucleation on Venus, given the low H_2O mixing ratio around 1 ppmv, the isothermal coefficient will be close to 1 and thus have a minimal effect on the nucleation rate (Määttänen et al., 2005). Using the lowest value of 0.966 reported by Määttänen et al. (2005) for H_2O in the comparable case of Mars, increases the nucleation activation temperature by <0.1 K. Using the lowest non-isothermal value of 0.006 reported for CO_2 ice nucleation (also for Mars) from Wood (1999), still only causes an approximate 0.3 K increase.

Z_{hom} is the homogeneous Zeldovich factor that accounts for the decrease in the rate of cluster formation when there is a finite rate of critical cluster formation and is defined as

$$Z_{hom} = \sqrt{\frac{\Delta F^*_{hom}}{3\pi kT n^{*2}}} \tag{A4}$$

Where n^* is the number of molecules in the critical cluster. β_{hom} describes the rate at which monomers collide with the cluster and is defined as

$$\beta_{hom} = c_{1,v} 4\pi r^{*2} \sqrt{\frac{kT}{2\pi m_m}} \tag{A5}$$

where m_m is the molar mass.

A2. Heterogeneous Nucleation

The rate of heterogeneous nucleation induced via surface diffusion on a spherical nucleus (J_{het}, a per nucleating particle nucleation rate in units of s^{-1}) is given by

$$J_{het} = A_N f_{\delta T} Z_{het} \beta_{het} c_{1,s} \exp\left(\frac{-\Delta F^*_{het}}{kT}\right) \tag{A6}$$

where A_N is the surface area of the INP and $c_{1,s}$ is the concentration of monomers on the particle surface; β_{het} describes the diffusion of molecules on the particle surface, and the dissociation of a proportion of supercritical clusters is described by the heterogeneous Zeldovich factor Z_{het}. ΔF_{het} is the free energy of forming a critical cluster on the nucleating particle, given by

$$\Delta F^*_{het} = f(m, x)\frac{16\pi\sigma^3 v^2}{3(kT \ln S)^2} \tag{A7}$$

ΔF^*_{het} is calculated relative to the homogeneous barrier (ΔF^*_{hom}) with a reduction in the energy barrier by a factor $f(m,x)$ as described in Fletcher (1958), where x is the ratio of the size of the nucleating particle to the size of the critical cluster and m is the contact parameter (equal to $\cos\theta$, where θ is the contact angle between the INP and the nucleating phase (pertinent values of θ are discussed in the following section).

There are significant uncertainties associated with the physical properties of CO_2 and H_2O under the extremely low temperatures in Venus's upper atmosphere. Hence, any predictions with CNT need to be taken in the context of these large uncertainties that propagate through the nucleation rate. For the CNT formulations in this paper we have used a combination of physical properties used in previous nucleation studies and values derived from recent experimental data. The physical properties used in this study are detailed in Table A1. In the cases where physical properties were derived or there was a choice, the methodology and discussion is given below.

Amorphous solid water: The homogeneous nucleation of ASW was determined assuming a water mixing ratio of 1 ppm and the saturation vapor pressure was defined by Nachbar et al. (2018, 2019). In the past the parameterization for the saturation pressure from Murphy and Koop (2005), where ASW and supercooled water were assumed to be a single continuous phase, had been used. However, Nachbar et al. (2019) showed that ASW and supercooled water are two distinct phases of water and have distinct thermodynamics. Nachbar et al. (2018)

showed that the vapor pressure of ASW is substantially greater than that predicted by the parameterization given by Murphy and Koop (2005). Surface tension of ASW is not directly measured in the literature, and we used a value that we derived from literature data for the adsorption of ASW on MSPs (Duft et al., 2019); we discuss this derivation in the heterogeneous section below. We set the non-isothermal constant to unity, which is probably an overestimate, but since we are attempting to identify which mechanisms are possible, introducing a highly uncertain term that would reduce the rate would not be helpful.

Using a two-structure model of water (Hruby & Holten, 2004) produces a surface tension value of $\sim$0.095 J m^{-2} for water in the temperature regime associated with Venus' upper mesosphere. Interestingly, they suggest that the temperature dependence of this value below $\sim$120 K is weak. In a study where the adsorption of ASW onto MSP particles was studied between 128 and 147 K, Duft et al. (2019) found that the surface tension was 0.094 ± 0.011 J m^{-2}. In order to derive a surface tension that was consistent with our CNT formulation we fitted to the data presented in Duft et al. (2019). They report critical supersaturations where adsorption of water leads to ice-activation. We interpreted the saturation at which we see a step change in the nucleation rate as being equivalent to the critical supersaturation reported by Duft et al. (2019). The nucleation rate is very sensitive to the desorption energy and we have used an average value of 42 kJ mol^{-1} which is in the range reported by Duft et al. (2019) for different MSP materials. This desorption energy is somewhat larger than that used by Määttänen et al. (2005) and reflects the strong binding of water molecules to the polar MSP surface. Given that the critical cluster is only a few 10s of molecules in size, the assumption that all these molecules experience an enhanced interaction with the surface is reasonable (Duft et al., 2019). We also follow Duft et al. (2019) in assuming that the MSP is wetted by ASW with m of 0.999. We fitted to reproduce the critical supersaturations in their Figure 6, yielding a surface tension of 0.085 J m^{-2}, which is within the uncertainty of the values reported by Duft et al. (2019). By constraining our CNT formulation to experimental data down to 120 K, we can have some confidence in the extrapolation to $\sim$110 K where we predict nucleation in Venus' atmosphere.

Liquid CO$_2$: It is not immediately obvious that liquid CO_2 should play any role in the atmosphere of Venus, since bulk liquid CO_2 can only exist at much greater pressures. However, recent experiments and computational studies have demonstrated that the initial cluster formed via homogeneous nucleation has liquid-like properties at temperatures pertinent to the upper atmosphere of Venus (Dingilian et al., 2020; Halonen et al., 2021). In order to produce a CNT formulation that is consistent with the nucleation rate (and supersaturation) data presented in Dingilian et al. (2020), we fitted the surface tension to the nucleation rate data between 78 and 92 K. The average was 0.0378 ± 0.0014 J m^{-2}. Dingilian et al. (2020) fitted their data using a parameterization for surface tension based on high-temperature data that was then extrapolated to the low temperatures of their experiments, producing values of 0.050–0.054 J m^{-2}. While there are uncertainties in these physical quantities, the pairing of the surface tension with our formulation of CNT to reproduce the experimentally observed nucleation rates under conditions close to those where clouds may form in Venus' upper mesosphere gives us some confidence in our results.

Appendix B: Rate Coefficients for Attachment and Detachment of CO$_2$ Molecules to MgCO$_3$(CO$_2$)$_n$ Clusters

Rate coefficients for the sequential addition of CO_2 molecules to $MgCO_3(CO_2)_3$, up to $MgCO_3(CO_2)_{40}$, were calculated using RRKM theory, using a solution of the Master Equation based on the inverse Laplace transform method (De Avillez Pereira et al., 1997). These $MgCO_3(CO_2)_n + CO_2$ recombination reactions proceed via the formation of an excited adduct, which can either dissociate back to reactants or be stabilized by collision with a third body to form $MgCO_3(CO_2)_{n+1}$. The binding energy of each CO_2 to the cluster was fixed at 26.6 kJ mol^{-1}, which is the heat of sublimation of CO_2 at 0 K (Chicko, 2022; Giauque & Egan, 1937). The internal energy of the adduct was divided into a contiguous set of grains with a width of 12 cm^{-1} (which reflects the small binding energy of CO_2 to the cluster), each containing a bundle of rovibrational states.

The density of states of the adduct was calculated using the Beyer−Swinehart algorithm (Gilbert & Smith, 1990) for the vibrational modes (without making a correction for anharmonicity). For each $MgCO_3(CO_2)_n$ cluster these modes were taken to consist of the vibrational modes of $MgCO_3$ (167, 490, 530, 673, 806, 826, 903, 990, 1,768 cm^{-1}) and the n CO_2 ligands (676, 676, 1,364, 2,400 cm^{-1} for each CO_2), calculated at the

B3LYP/6–311 + g(2d,p) level of theory (Frisch et al., 2016) and assumed to be independent of each other; and further $5n$ low-frequency modes set to a frequency of 80 cm^{-1}. This frequency represents the geometric mean of the frequencies of the "new" vibrational modes that are created when n CO_2 molecules cluster with $MgCO_3$. The actual geometric means for $n = 2$, 3, and 4 are 75.1, 83.2, and 78.5 cm^{-1}, respectively, using the data in Table S3 in the Supporting Information of Plane et al. (2018). The geometric mean is used because the density of states of the cluster is proportional to the inverse product of the vibrational frequencies (Gilbert & Smith, 1990). Classical densities of states treatment was used for the rotational modes. Since the clusters will be approximately spherical as they grow, the moments of inertia were approximated to be that of a solid sphere about its diameter:

$$I = 0.4Mr^2 \tag{B1}$$

where M is the mass of the cluster and r is the cluster radius assuming a density of 1,562 kg m^{-3} for solid CO_2 at 195 K.

Each grain associated with the adduct $MgCO_3(CO_2)_{n+1}$ was then assigned a set of microcanonical rate coefficients for dissociation back to $MgCO_3(CO_2)_n$ + CO_2. These rate coefficients are determined using inverse Laplace transformation to link them directly to $k_{rec,\infty}$, which is estimated here as the hard sphere collision frequency between $MgCO_3(CO_2)_n$ and CO_2, with a small $T^{1/2}$ temperature dependence (Smith, 1980). The probability of collisional transfer between grains was estimated using the exponential down model, where the average energy for downward transitions $\langle \Delta E \rangle_{down}$ was set to 600 cm^{-1} which is typical of M = CO_2 at 300 K, and treated as independent of temperature (Gilbert & Smith, 1990). The Master Equation, which describes the evolution with time of the grain populations of the adduct, was then expressed in matrix form and solved to yield the rate coefficients for sequential addition of CO_2 to the clusters, as a function of temperature (50–150 K) at a pressure of 10^{-5} Torr, which is the typical pressure at ~150 km in Venus' atmosphere (Mahieux et al., 2015).

For the purpose of atmospheric modeling, it is customary to use the uptake coefficient, γ. This was calculated as the ratio of the recombination rate coefficient to the collision rate of CO_2 with a sphere of radius r:

$$\gamma = \frac{k_{rec}[CO_2]}{(0.25\overline{c}A)} \tag{B2}$$

where k_{rec} is the recombination rate coefficient, $\overline{c}$ is the mean collision speed between $MgCO_3(CO_2)_n$ and CO_2, and A is the surface area of the cluster ($4\pi r^2$). γ is illustrated as a function of n and T in Figure B1a. Note that γ does not exceed unity, which is a good test of the Master Equation calculation.
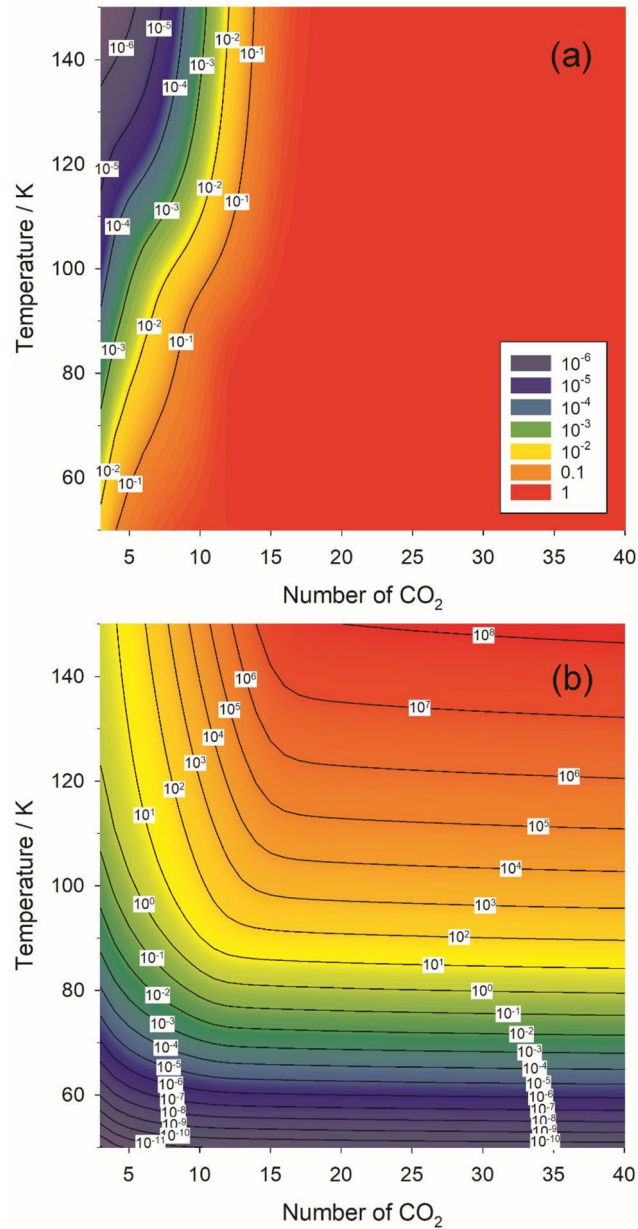
Figure B1. (a) γCO_2 as a function of temperature and number of CO_2 molecules clustered around a meteoric smoke particle. (b) Rate of evaporation (units: molecule s^{-1}) of CO_2 from a Meteoric Smoke Particle-$(CO_2)_n$ cluster, as a function of temperature and the number of CO_2 molecules (n).

Finally, the rate of dissociation of the cluster that is, $MgCO_3(CO_2)_{n+1} \rightarrow MgCO_3(CO_2)_n + CO_2$, was calculated using detailed balance with the recombination rate coefficient, where the equilibrium constant is calculated using statistical mechanics with the partition functions for $MgCO_3(CO_2)_{n+1}$ and $MgCO_3(CO_2)_n$ using the vibrational frequencies and rotational constants described above. The equilibrium constant is within 20% of that given by the Antoine relation (Chicko, 2022; Giauque & Egan, 1937) for clusters larger than $n = 30$ and $T > 140$ K (where the Antoine relation is valid). The dissociation rate, that is, the evaporation rate, is shown as a function of n and T in Figure B1b.

Appendix C: Details of the Microphysical Model

In order to explore the evolution of the CO_2-ice clouds, a 1-dimensional model was constructed which describes the nucleation, growth, sedimentation, and sublimation of the ice particles. For this simple cloud model, we describe the production of CO_2 particles using the KNT theory presented in Section 2.4. Hence, we implicitly assume that nucleation occurs on MSP, probably $MgCO_3$ and $FeCO_3$. Although we expect very similar results in terms of growth, sedimentation and lifetime of cloud particles if nucleation occurs on ASW particles which in turn nucleate on MSPs.

When the concentration of MSPs is larger than $\sim1,000$ cm^{-3}, the production of large CO_2 particles with radii of a few hundred nm starts to deplete significantly the background CO_2 density (this effect is accounted for in the model). Because the CO_2 ice clouds are short-lived, coagulation of ice particles is neglected.

The sedimentation velocity of the $MgCO_3(CO_2)_n$ clusters and CO_2 ice particles, w_i, can be estimated using a form of Stokes' law describing a spherical particle falling through a stationary fluid:

$$w_i = \frac{2(\rho_p - \rho_{air})}{9\mu} g \, r_i^2 C_{scf} \tag{C1}$$

where ρ_p and ρ_{air} are the particle density (taken to be the density for solid CO_2, which is 1,562 kg m^{-3} at 195 K) and the air density, respectively; μ is the dynamic viscosity of CO_2 at the atmospheric temperature and pressure; g is the gravitational constant (8.87 m s^{-2} for Venus); and r_i is the particle radius. C_{scf} is the Cunningham slip correction factor accounting for the effects of drag on small particles, and is estimated from Equation B2, where λ is the mean free path of the CO_2 molecules, and A_1, A_2, and A_3 are dimensionless coefficients:

$$C_{scf} = 1 + \frac{\lambda}{r_i}\left(A_1 + A_2 \exp\left(\frac{-A_3 r_i}{\lambda}\right)\right) \tag{C2}$$

Data Availability Statement

We have included all relevant equations and physical quantities to reproduce the plots in this paper in the appendices. In addition, the codes, spreadsheets, and data to reproduce the plots in this manuscript are available (Murray et al., 2023). The SOIR temperature profiles we used were from Mahieux et al. (2015). The profiles can be found in the Virtual European Solar and Planetary Access database (https://vespa-client-dev.obspm.fr/planetary/data/) and the profile data set is described in Trompet et al. (2018). The Mie calculations were done using the MiePlot v4.6.14 application interface (http://www.philiplaven.com/mieplot.htm).

References

Azreg-Aïnou, M. (2005). Low-temperature data for carbon dioxide. *Monatshefte für Chemie*, *136*(12), 2017–2027. https://doi.org/10.1007/s00706-005-0370-3

Bottema, M., Plummer, W., Strong, J., & Zander, R. (1965). The composition of the Venus clouds and implications for model atmospheres. *Journal of Geophysical Research*, *70*(17), 4401–4402. https://doi.org/10.1029/JZ070i017p04401

Bromley, S. T., Gómez Martín, J. C., & Plane, J. M. C. (2016). Under what conditions does (SiO)N nucleation occur? A bottom-up kinetic modelling evaluation. *Physical Chemistry Chemical Physics*, *18*(38), 26913–26922. https://doi.org/10.1039/C6CP03629E

Carrillo-Sánchez, J. D., Gómez-Martín, J. C., Bones, D. L., Nesvorný, D., Pokorný, P., Benna, M., et al. (2020). Cosmic dust fluxes in the atmospheres of Earth, Mars, and Venus. *Icarus*, *335*, 113395. https://doi.org/10.1016/j.icarus.2019.113395

Chamberlain, S., Mahieux, A., Robert, S., Piccialli, A., Trompet, L., Vandaele, A. C., & Wilquet, V. (2020). SOIR/VEx observations of water vapor at the terminator in the Venus mesosphere. *Icarus*, *346*, 113819. https://doi.org/10.1016/j.icarus.2020.113819

Chicko, J. S. (2022). Heat of sublimation data. In P. J. Linstrom & W. G. Mallard (Eds.), *NIST chemistry WebBook, NIST standard reference database number 69* (p. 20899). National Institute of Standards and Technology.

Clancy, R. T., Wolff, M. J., Smith, M. D., Kleinböhl, A., Cantor, B. A., Murchie, S. L., et al. (2019). The distribution, composition, and particle properties of Mars mesospheric aerosols: An analysis of CRISM visible/near-IR limb spectra with context from near-coincident MCS and MARCI observations. *Icarus*, *328*, 246–273. https://doi.org/10.1016/j.icarus.2019.03.025

De Avillez Pereira, R., Baulch, D. L., Pilling, M. J., Robertson, S. H., & Zeng, G. (1997). Temperature and pressure dependence of the multichannel rate coefficients for the CH_3+ OH system. *The Journal of Physical Chemistry A*, *101*(50), 9681–9693. https://doi.org/10.1021/jp972140+

Ding, J., Yang, P., Lemmon, M. T., & Zhang, Y. (2023). Simulations of halos produced by carbon dioxide ice crystals in the Martian atmosphere. *Geophysical Research Letters*, *50*(8), e2023GL103457. https://doi.org/10.1029/2023GL103457

Dingilian, K. K., Halonen, R., Tikkanen, V., Reischl, B., Vehkamäki, H., & Wyslouzil, B. E. (2020). Homogeneous nucleation of carbon dioxide in supersonic nozzles I: Experiments and classical theories. *Physical Chemistry Chemical Physics*, *22*(34), 19282–19298. https://doi.org/10.1039/D0CP02279A

Duft, D., Nachbar, M., & Leisner, T. (2019). Unravelling the microphysics of polar mesospheric cloud formation. *Atmospheric Chemistry and Physics*, *19*(5), 2871–2879. https://doi.org/10.5194/acp-19-2871-2019

Feder, J., Russell, K. C., Lothe, J., & Pound, G. M. (1966). Homogeneous nucleation and growth of droplets in vapours. *Advances in Physics*, *15*(57), 111–178. https://doi.org/10.1080/00018736600101264

Fedorova, A. A., Montmessin, F., Korablev, O., Luginin, M., Trokhimovskiy, A., Belyaev, D. A., et al. (2020). Stormy water on Mars: The distribution and saturation of atmospheric water during the dusty season. *Science*, *367*(6475), 297–300. https://doi.org/10.1126/science.aay9522

Fletcher, N. H. (1958). Size effect in heterogeneous nucleation. *The Journal of Chemical Physics*, *29*(3), 572–576. https://doi.org/10.1063/1.1744540

Frisch, M. J., Trucks, G. W., Schlegel, H. B., Scuseria, G. E., Robb, M. A., Cheeseman, J. R., et al. (2016). *Gaussian 16, revision B.01*. Gaussian, Inc.

Gérard, J. C., Cox, C., Saglam, A., Bertaux, J. L., Villard, E., & Nehmé, C. (2008). Limb observations of the ultraviolet nitric oxide nightglow with SPICAV on board Venus express. *Journal of Geophysical Research*, *113*(E5), E00B03. https://doi.org/10.1029/2008JE003078

Ghormley, J. A., & Hochanadel, C. J. (1971). Amorphous ice: Density and reflectivity. *Science*, *171*(3966), 62–64. https://doi.org/10.1126/science.171.3966.62

Giauque, W. F., & Egan, C. J. (1937). Carbon dioxide. The heat capacity and vapor pressure of the solid. The heat of sublimation. Thermodynamic and spectroscopic values of the entropy. *The Journal of Chemical Physics*, *5*(1), 45–54. https://doi.org/10.1063/1.1749929

Gilbert, R. G., & Smith, S. C. (1990). Theory of unimolecular and recombination reactions.

Glandorf, D. L., Colaprete, A., Tolbert, M. A., & Toon, O. B. (2002). CO_2 snow on Mars and early Earth: Experimental constraints. *Icarus*, *160*(1), 66–72. https://doi.org/10.1006/icar.2002.6953

Hale, B. N., & Plummer, P. L. M. (1974). On nucleation phenomena I: A molecular model. *Journal of the Atmospheric Sciences*, *31*(6), 1615–1621. https://doi.org/10.1175/1520-0469(1974)031<1615:ONPIAM>2.0.CO;2

Halonen, R., Tikkanen, V., Reischl, B., Dingilian, K. K., Wyslouzil, B. E., & Vehkamäki, H. (2021). Homogeneous nucleation of carbon dioxide in supersonic nozzles II: Molecular dynamics simulations and properties of nucleating clusters. *Physical Chemistry Chemical Physics*, *23*(8), 4517–4529. https://doi.org/10.1039/D0CP05653G

Hansen, G. B. (1997). The infrared absorption spectrum of carbon dioxide ice from 1.8 to 333 μm. J*ournal of Geophysical Research*, *102*(E9), 21569–21587. https://doi.org/10.1029/97je01875

Hansen, G. B. (2005). Ultraviolet to near-infrared absorption spectrum of carbon dioxide ice from 0.174 to 1.8 μm. *Journal of Geophysical Research*, *110*(E11), E11003. https://doi.org/10.1029/2005je002531

Hervig, M. E., Plane, J. M. C., Siskind, D. E., Feng, W., Bardeen, C. G., & Bailey, S. M. (2021). New global meteoric smoke observations from SOFIE: Insight regarding chemical composition, meteoric influx, and hemispheric asymmetry. *Journal of Geophysical Research: Atmospheres*, *126*(13), e2021JD035007. https://doi.org/10.1029/2021jd035007

Hruby, J., & Holten, V. (2004). A two-structure model of thermodynamic properties and surface tension of supervooled water. In *Proceedings of the 14th international conference on the properties of water and steam*. Maruzen.

Kofman, V., He, J., Loes ten Kate, I., & Linnartz, H. (2019). The refractive index of amorphous and crystalline water ice in the UV–vis. *The Astrophysical Journal*, *875*(2), 131. https://doi.org/10.3847/1538-4357/ab0d89

Limaye, S. S., Grassi, D., Mahieux, A., Migliorini, A., Tellmann, S., & Titov, D. (2018). Venus atmospheric thermal structure and radiative balance. *Space Science Reviews*, *214*(5), 102. https://doi.org/10.1007/s11214-018-0525-2

Listowski, C., Määttänen, A., Montmessin, F., Spiga, A., & Lefevre, F. (2014). Modeling the microphysics of CO_2 ice clouds within wave-induced cold pockets in the martian mesosphere. *Icarus*, *237*, 239–261. https://doi.org/10.1016/j.icarus.2014.04.022

Listowski, C., Määttänen, A., Riipinen, I., Montmessin, F., & Lefevre, F. (2013). Near-pure vapor condensation in the martian atmosphere: CO_2 ice crystal growth. *Journal of Geophysical Research: Planets*, *118*(10), 2153–2171. https://doi.org/10.1002/jgre.20149

Lübken, F. J., Lautenbach, J., Höffner, J., Rapp, M., & Zecha, M. (2009). First continuous temperature measurements within polar mesosphere summer echoes. *Journal of Atmospheric and Solar-Terrestrial Physics*, *71*(3–4), 453–463. https://doi.org/10.1016/j.jastp.2008.06.001

Luginin, M., Fedorova, A., Belyaev, D., Montmessin, F., Wilquet, V., Korablev, O., et al. (2016). Aerosol properties in the upper haze of Venus from SPICAV IR data. *Icarus*, *277*, 154–170. https://doi.org/10.1016/j.icarus.2016.05.008

Määttänen, A., Vehkamaki, H., Lauri, A., Merikallio, S., Kauhanen, J., Savijarvi, H., & Kulmala, M. (2005). Nucleation studies in the Martian atmosphere. *Journal of Geophysical Research*, *110*(E2), E02002. https://doi.org/10.1029/2004je002308

Määttänen, A., Vehkamaki, H., Lauri, A., Napari, I., & Kulmala, M. (2007). Two-component heterogeneous nucleation kinetics and an application to Mars. *Journal of Chemical Physics*, *127*(13), 134710. https://doi.org/10.1063/1.2770737

Mahieux, A., Robert, S., Piccialli, A., Trompet, L., & Vandaele, A. C. (2023). The SOIR/Venus express species concentration and temperature database: CO_2, CO, H_2O, HDO, $H_{35}Cl$, $H_{37}Cl$, HF individual and mean profiles. *Icarus*, *405*, 115713. https://doi.org/10.1016/j.icarus.2023.115713

Mahieux, A., Vandaele, A., Bougher, S., Drummond, R., Robert, S., Wilquet, V., et al. (2015). Update of the Venus density and temperature profiles at high altitude measured by SOIR on board Venus Express. *Planetary and Space Science*, *113–114*, 309–320. https://doi.org/10.1016/j.pss.2015.02.002

Mangan, T. P., Frankland, V. L., Murray, B. J., & Plane, J. M. C. (2017). The fate of meteoric metals in ice particles: Effects of sublimation and energetic particle bombardment. *Journal of Atmospheric and Solar-Terrestrial Physics*, *161*, 143–149. https://doi.org/10.1016/j.jastp.2017.07.002

Mangan, T. P., Plane, J. M. C., & Murray, B. J. (2021). The phase of water ice which forms in cold clouds in the mesospheres of Mars, Venus, and Earth. *Journal of Geophysical Research: Planets*, *126*(3), e2020JE006796. https://doi.org/10.1029/2020JE006796

Mangan, T. P., Salzmann, C. G., Plane, J. M. C., & Murray, B. J. (2017). CO_2 ice structure and density under Martian atmospheric conditions. *Icarus*, *294*, 201–208. https://doi.org/10.1016/j.icarus.2017.03.012

Menzel, D. H., & Whipple, F. L. (1954). The case for H_2O clouds on Venus. *The Astronomical Journal*, *59*, 329. https://doi.org/10.1086/107037

Michels, A., Wassenaar, T., Zwietering, T., & Smits, P. (1950). The vapour pressure of liquid carbon dioxide. *Physica*, *16*(5), 501–504. https://doi.org/10.1016/0031-8914(50)90135-2

Montmessin, F., Bertaux, J. L., Quémerais, E., Korablev, O., Rannou, P., Forget, F., et al. (2006). Subvisible CO_2 ice clouds detected in the mesosphere of Mars. *Icarus*, *183*(2), 403–410. https://doi.org/10.1016/j.icarus.2006.03.015

Mullin, J. W. (2001). *Crystallization*. Elsevier.

Murphy, D. M., & Koop, T. (2005). Review of the vapour pressures of ice and supercooled water for atmospheric applications. *Quarterly Journal of the Royal Meteorological Society*, *131*(608), 1539–1565. https://doi.org/10.1256/qj.04.94

Murray, B. J., & Jensen, E. J. (2010). Homogeneous nucleation of amorphous solid water particles in the upper mesosphere. *Journal of Atmospheric and Solar-Terrestrial Physics*, *72*(1), 51–61. https://doi.org/10.1016/j.jastp.2009.10.007

Murray, B. J., & Plane, J. M. C. (2003). The uptake of atomic oxygen on ice films: Implications for noctilucent clouds. *Physical Chemistry Chemical Physics*, *5*(19), 4129–4138. https://doi.org/10.1039/B305555H

Murray, B. J., & Plane, J. M. C. (2005). Modelling the impact of noctilucent cloud formation on atomic oxygen and other minor constituents of the summer mesosphere. *Atmospheric Chemistry and Physics*, *5*(4), 1027–1038. https://doi.org/10.5194/acp-5-1027-2005

Murray, B. J., Plane, J. M. C., Mangan, T. P., & Määttänen, A. (2023). Data and codes associated with 'ephemeral ice clouds in the upper mesosphere of Venus'. https://doi.org/10.5518/1375

Nachbar, M., Duft, D., & Leisner, T. (2018). The vapor pressure over nano-crystalline ice. *Atmospheric Chemistry and Physics*, *18*(5), 3419–3431. https://doi.org/10.5194/acp-18-3419-2018

Nachbar, M., Duft, D., & Leisner, T. (2019). The vapor pressure of liquid and solid water phases at conditions relevant to the atmosphere. *The Journal of Chemical Physics*, *151*(6), 064504. https://doi.org/10.1063/1.5100364

Nachbar, M., Duft, D., Mangan, T. P., Martin, J. C. G., Plane, J. M. C., & Leisner, T. (2016). Laboratory measurements of heterogeneous CO_2 ice nucleation on nanoparticles under conditions relevant to the Martian mesosphere. *Journal of Geophysical Research: Planets*, *121*(5), 753–769. https://doi.org/10.1002/2015JE004978

Palen, S., Kay, L., Smith, B., & Blumenthal, G. (2019). *Understanding our universe* (3rd ed.). W. W. Norton & Co.

Plane, J. M. C., Carrillo-Sanchez, J. D., Mangan, T. P., Crismani, M. M. J., Schneider, N. M., & Määttänen, A. (2018). Meteoric metal chemistry in the martian atmosphere. *Journal of Geophysical Research: Planets*, *123*(3), 695–707. https://doi.org/10.1002/2017je005510

Plane, J. M. C., Feng, W., & Dawkins, E. C. M. (2015). The mesosphere and metals: Chemistry and changes. *Chemical Reviews*, *115*(10), 4497–4541. https://doi.org/10.1021/cr500501m

Plane, J. M. C., Saunders, R. W., Hedin, J., Stegman, J., Khaplanov, M., Gumbel, J., et al. (2014). A combined rocket-borne and ground-based study of the sodium layer and charged dust in the upper mesosphere. *Journal of Atmospheric and Solar-Terrestrial Physics*, *118*, 151–160. https://doi.org/10.1016/j.jastp.2013.11.008

Pollack, J. B., & Sagan, C. (1968). The case for ice clouds. *Venus*, *73*(18), 5943–5949. https://doi.org/10.1029/JB073i018p05943

Pruppacher, H. R., & Klett, J. D. (1997). *Microphysics of clouds and precipitation*. Kluwer Academic Publishers. Retrieved from http://site.ebrary.com/id/10067306

Rea, D. G., & O'Leary, B. T. (1968). On the composition of the Venus clouds. *On the composition of the Venus clouds*, *73*(2), 665–675. https://doi.org/10.1029/JB073i002p00665

Saunders, R. W., Möhler, O., Schnaiter, M., Benz, S., Wagner, R., Saathoff, H., et al. (2010). An aerosol chamber investigation of the heterogeneous ice nucleating potential of refractory nanoparticles. *Atmospheric Chemistry and Physics*, *10*(3), 1227–1247. https://doi.org/10.5194/acp-10-1227-2010

Seki, J., & Hasegawa, H. (1983). The heterogeneous condensation of interstellar ice grains. *Astrophysics and Space Science*, *94*(1), 177–189. https://doi.org/10.1007/BF00651770

Smith, I. W. M. (1980). *Kinetics and dynamics of elementary gas reactions*. Butterworths.

Span, R., & Wagner, W. (1996). A new equation of state for carbon dioxide covering the fluid region from the triple-point temperature to 1100 K at pressures up to 800 MPa. *Journal of Physical and Chemical Reference Data*, *25*(6), 1509–1596. https://doi.org/10.1063/1.555991

Stcherbinine, A., Vincendon, M., Montmessin, F., Wolff, M. J., Korablev, O., Fedorova, A., et al. (2020). Martian water ice clouds during the 2018 global dust storm as observed by the ACS-MIR channel onboard the trace gas orbiter. *Journal of Geophysical Research: Planets*, *125*(3), e2019JE006300. https://doi.org/10.1029/2019JE006300

Takagi, S., Mahieux, A., Wilquet, V., Robert, S., Vandaele, A. C., & Iwagami, N. (2019). An uppermost haze layer above 100 km found over Venus by the SOIR instrument onboard Venus Express. *Earth Planets and Space*, *71*(1), 124. https://doi.org/10.1186/s40623-019-1103-x

Titov, D. V., Ignatiev, N. I., McGouldrick, K., Wilquet, V., & Wilson, C. F. (2018). Clouds and hazes of Venus. *Space Science Reviews*, *214*(8), 126. https://doi.org/10.1007/s11214-018-0552-z

Trompet, L., Geunes, Y., Ooms, T., Mahieux, A., Wilquet, V., Chamberlain, S., et al. (2018). Description, accessibility and usage of SOIR/Venus express atmospheric profiles of Venus distributed in VESPA (virtual European solar and planetary access). *Planetary and Space Science*, *150*, 60–64. https://doi.org/10.1016/j.pss.2017.04.022

Turco, R. P., Toon, O. B., Whitten, R. C., & Keesee, R. G. (1983). Venus: Mesospheric hazes of ice, dust, and acid aerosols. *Icarus*, *53*(1), 18–25. https://doi.org/10.1016/0019-1035(83)90017-9

Warren, S. G. (1986). Optical constants of carbon dioxide ice. *Applied Optics*, *25*(16), 2650–2674. https://doi.org/10.1364/AO.25.002650

Warren, S. G., & Brandt, R. E. (2008). Optical constants of ice from the ultraviolet to the microwave. *A Revised Compilation*, *113*(D14), 1206–1225. https://doi.org/10.1029/2007JD009744

Wilquet, V., Drummond, R., Mahieux, A., Robert, S., Vandaele, A. C., & Bertaux, J.-L. (2012). Optical extinction due to aerosols in the upper haze of Venus: Four years of SOIR/VEX observations from 2006 to 2010. *Icarus*, *217*(2), 875–881. https://doi.org/10.1016/j.icarus.2011.11.002

Wilquet, V., Fedorova, A., Montmessin, F., Drummond, R., Mahieux, A., Vandaele, A. C., et al. (2009). Preliminary characterization of the upper haze by SPICAV/SOIR solar occultation in UV to mid-IR onboard Venus Express. *Journal of Geophysical Research*, *114*(E9), E00B42. https://doi.org/10.1029/2008JE003186

Wölk, J., Wyslouzil, B. E., & Strey, R. (2013). Homogeneous nucleation of water: From vapor to supercooled droplets to ice. *AIP Conference Proceedings*, *1527*(1), 55–62. https://doi.org/10.1063/1.4803203

Wood, S. E. (1999). *Nucleation and growth of carbon dioxide ice crystals in the Martian atmosphere*. Ph.D., University of California.